Towards the dehydration of ethanol using pervaporation cross-linked poly(vinyl alcohol)/graphene oxide membranes

Roberto Castro-Muñoz[a, b, c], Juan Buera-González[a], Óscar de la Iglesia[a, d], Francesco Galiano[b], Vlastimil Fíla[c], Magdalena Malankowska[a], César Rubio[a], Alberto Figoli[b], Carlos Téllez[a], Joaquín Coronas[a,*]

(a) Chemical and Environmental Engineering Department, Instituto de Nanociencia de Aragón (INA) and Instituto de Ciencia de Materiales de Aragón (ICMA), Universidad de Zaragoza-CSIC, 50018 Zaragoza, Spain. Email: coronas@unizar.es

(b) Institute on Membrane Technology, ITM-CNR, c/o University of Calabria, P. Bucci 17c, 87030 Rende (CS), Italy

(c) University of Chemistry and Technology Prague, Technická 5, 166 28 Prague 6, Czech Republic

(d) Centro Universitario de la Defensa Zaragoza, Academia General Militar, 50090 Zaragoza, Spain

Abstract

Highly hydrophilic inorganic material graphene oxide (GO) was successfully prepared and incorporated into a cross-linked poly(vinyl alcohol) (PVA) matrix. The obtained mixed matrix membranes (MMMs) have been used for the dehydration of ethanol (10:90% water-ethanol) by pervaporation (PV), monitoring their performance in terms of total permeate flux, partial components fluxes, as well as their separation factor. The effect of filler was analyzed by doubling the GO content (at 0.5, 1.0, and 2.0 wt.%) in the MMMs.

A complete analysis of the operating temperature (between 40-70 ºC) was carried out by means of Arrhenius relationship. Moreover, the membranes were characterized by field emission scanning electron microscopy (FESEM), transmission electron microscopy (TEM), differential scanning calorimetry (DSC), thermo-gravimetric analysis (TGA), X-ray diffraction (XRD), Fourier transformed infrared spectroscopy (FTIR), measurements of degree of swelling (uptake), water contact angle (CA) and mechanical properties. At 40 ºC, the best performance was provided by the MMMs containing 1 wt.% GO, showing a separation factor of 263 and a permeate flux of about 0.137 $kg \cdot m^{-2} \cdot h^{-1}$ (in which 0.133 $kg \cdot m^{-2} \cdot h^{-1}$ corresponds to water). This represents a 75 % enhancement of the original permeation rate of pristine cross-linked PVA membranes. Taking into account the promising results, it is likely that these MMMs will provide featured benefits in green processes, e.g. ethanol purification by means of less-energy consumption.

Keywords: pervaporation; poly (vinyl alcohol); cross-linking; mixed matrix membrane; ethanol dehydration; graphene oxide.

Nomenclature

PV: Pervaporation
PVA: Poly(vinyl alcohol)
CA: water contact angle
J: Permeate flux, $kg \cdot m^{-2} \cdot h^{-1}$
α: Separation factor
FESEM: Field emission scanning electron microscopy
DSC: Differential scanning calorimetry
MMM: Mixed matrix membrane
TGA: Thermo-gravimetric analysis

GO: Graphene oxide

XRD: X-ray diffraction

1. Introduction

Membrane-based technologies have attracted considerable attention for different types of applications (e.g. in food, petrochemical and environmental fields). In particular, pervaporation (PV), as a merge of evaporation and permeation processes, has been consistently proposed for the separation of different types of azeotropic and close-boiling compounds mixtures. The benefit of using this membrane process for such purposes is due to its high selectivity, efficiency and low-energy requirements [1,2]; the latest being the main feature of PV that indeed makes it attractive to be considered as a "Green" process. These mechanisms are currently encouraged to meet the "*Twelve Principles of Green Chemistry*". Such principles, well-established by Anastas and Warner [3], are aimed to preserve the environment through implementation of green chemistry methods. Moreover, PV is a good candidate for the replacement of the conventional distillation, which, for instance, carries out the separation of azeotropic mixtures at large-scale in petrochemical industry. PV has demonstrated the ability to separate different types of azeotropic mixtures, including organic-water, organic-organic and water-organic [4,5]. At industrial level, PV has found its growing use in industry towards water-organic mixtures, which implies the dehydration of organics to reach higher purification degrees, e.g. in ethanol [6], isopropanol [7] and acetonitrile [8]. To date, the dehydration of ethanol is the most sought application due to its direct impact on commercial value. According to the IEA (Industrial Ethanol Association, http://www.industrial-ethanol.org), the main market for ethanol concerns the manufacture of beverages, fuels and a multiple of industrial

applications related to pharmaceuticals, cosmetics, detergents, printing inks, paints, coatings, medical uses, production of polymers and chemicals, to mention just a few. This makes the ethanol production continuously grow, e.g. over 100 billion liters demand was reported by 2017 [9], and its demands is expected to increase in coming years. Typically, ethanol can be produced by fermentation or from direct hydration of ethylene. Moreover, regardless of its production process, the final product is usually a diluted aqueous solution and at a large-scale level, the ethanol is processed by distillation in order to concentrate it. The separation of ethanol and water is complicated due to the fact that ethanol and water form an azeotrope at 95.6 wt.% of ethanol [10]. Thereby, it is a difficult task to produce pure ethanol from an azeotropic mixture by conventional distillation: at the azeotrope vapor and liquid compositions are the same. Herein, the PV has been introduced as a promising alternative towards such purpose. When dealing with the dehydration of any organic (e.g. ethanol), it is inevitable to address the use of hydrophilic membranes. At this point, several types of hydrophilic polymers have been proposed and investigated as membrane materials, such as polyimides [6], sodium alginate [11], polybenzimidazole (PBI) [12], chitosan [13], polyacrylonitrile (PAN) [14] and poly(vinyl alcohol) (PVA) [7]. Among all these polymers, PVA has been the only one to be consolidated at industrial level. For instance, DeltaMem AG (http://www.deltamem.ch) is a company that currently manufactures and commercializes cross-linked PVA membranes for PV applications. Nowadays, one of the most successful trends in enhancing the performance of polymeric membranes implies the embedding of inorganic materials, generating the so-called mixed matrix membranes (MMMs). These combine the strengths of inorganic and polymeric membranes to ideally reach an enhanced

synergistic performance. To date, some MMMs based on PVA have been proposed for ethanol dehydration displaying acceptable separation performance, e.g. those containing MWCNT (J= 0.080 $kg \cdot m^{-2} \cdot h^{-1}$, α=500) [15] and ZIF-8-$NH_2$ (J=0.120 $kg \cdot m^{-2} \cdot h^{-1}$, α=200) [16]. In this work, the possibility of incorporating a highly hydrophilic material, like graphene oxide (GO), into cross-linked PVA membranes, to achieve better performance, was studied. GO is a layered material produced by the oxidation of graphite. GO sheets are highly oxygenated having hydroxyl and epoxy functional groups on their basal planes, in addition to carbonyl and carboxyl groups located at the sheet edges. These functional groups provide a high hydrophilic profile to the material [17], which has been noted in PVA during organic-organic separations [18,19]. Thereby, the aim of this work was to analyze the effect of GO on the performance of cross-linked PVA MMMs used in ethanol dehydration. To the best of our knowledge, there is no report about this [5]. The effect of operating temperature on total permeate flux and separation factor was investigated by doubling the GO content (at 0.5, 1.0, and 2.0 wt.%) in the MMMs. Moreover, the pristine membrane and MMMs were characterized by thermogravimetric analysis (TGA), differential scanning calorimetry (DSC), field emission scanning electron microscopy (FESEM), transmission electron microscopy (TEM), degree of swelling (uptake), X-ray diffraction (XRD), Fourier transformed infrared spectroscopy (FTIR), measurements of water contact angle and mechanical properties.

2. Experimental

2.1. Materials

120 Poly (vinyl alcohol) (PVA, MW:130,000), glutaraldehyde (grade II, 25 wt.%) and
121 hydrochloric acid (HCl) were acquired from Sigma-Aldrich and used without further
122 purification.
123
124 *2.2. Synthesis of graphene oxide*
125 Graphene oxide (GO) was synthesized following the procedure described by Castarlenas
126 et al. [20], according to the Hummers' method [21]. Basically, the graphite is oxidized by
127 treatment with $KMnO_4$ and $NaNO_3$ in concentrated H_2SO_4. In a round bottom flask,
128 sodium nitrate (1.5 g) was dissolved in 70 mL of concentrated sulfuric acid. The dispersion
129 was put under stirring at room temperature until the $NaNO_3$ was totally dissolved
130 (approximately 5-10 min). Therefore, graphite (3.0 g) (with a particle size of ca. 5 μm,
131 supplied by Richard Anton KG) was added to the solution under gentle stirring for about
132 30 min to facilitate a homogeneous suspension. Later, $KMnO_4$ (9.0 g) was gradually
133 added to the suspension to avoid the increase of the flask temperature due to the heat
134 generated during redox reaction. Once the addition of $KMnO_4$ was completed, the
135 temperature of the solution was slowly raised up to 35 ºC and maintained for 30 min under
136 stirring. To facilitate the control of the exothermic reaction an ice bath was put under the
137 glass balloon. A brownish gray paste was formed. Then, by means of a Pasteur pipette,
138 140 mL of deionized water was slowly added to the slurry considering that the smoke
139 production was very fast. Once the deionized water was added, the suspension was kept
140 stirring overnight at 95 ºC and later, 500 mL of deionized water was added followed by
141 20 mL H_2O_2 that reduced the residual permanganate. The round bottom flask was kept
142 under stirring at 95 ºC for 3 h. The resulting mixture was filtered and washed using a 10

wt.% aqueous HCl solution. Finally, GO was centrifuged and washed with water 4 times at 10000 rpm for 15 min (Beckman Coulter, Allegra x-15 R), reaching the neutral pH, and dried at 80 ºC overnight obtaining 4.2 g of a light brown solid.

2.3. Mixed matrix membrane preparation

PVA/GO MMMs were prepared by dense-film casting method and solvent evaporation. PVA powder (3 g) was dissolved under stirring in 100 mL of distilled water at 90 ºC. The obtained solution was filtered to remove any insoluble impurities. GO was added to the PVA solution to produce the dope suspension that was stirred during 12 h and processed by sonication twice (30 min each). Afterwards, the in situ cross-linking procedure was performed by adding 0.1 mL of GA and 0.1 mL of HCl to the dope. This was stirred during 15 min, cast on a clean glass plate and then dried in an oven at 40 ºC during 2 days. Finally, the MMMs were peeled off of the glass plate. The GO loading for the MMMs was varied at 0.5, 1, and 2 wt.%. **Figure 1** shows typical examples of the prepared membranes for this study, with a membrane thickness of 40±2 μm (measured with digital micrometer Mitutoyo with an accuracy of 1 μm). It can be observed that the presence of GO particles provides a darker colour on the MMM surface.

Figure 1. Pure cross-linked PVA membrane and its MMMs-GO with 1 wt.% of filler.

2.3.1. Membrane characterization

Field emission scanning electron microscopy (FESEM). The morphological structure of the membrane surface and cross-section of the cross-linked-PVA and its MMMs were

166 evaluated using a field emission scanning electron microscope (FEI Inspect, F50
167 operated at 20 kV). The cross-sections were obtained by cryogenic fracture immersion of
168 the samples in liquid N_2. The samples were attached to SEM carbon stubs with a diameter
169 of 2.54 cm using two-sided adhesive tape. The samples were coated through a sputtering
170 process with gold-palladium (Au / Pd). The corresponding images were captured at
171 suitable magnification.
172 *Transmission electron microscopy (TEM)*. The distribution and dimensions of GO sheets
173 in cross-linked PVA-GO 1 wt.% membrane were obtained from TEM images (FEI TECNAI
174 T20 transmission microscope at 200 kV). The membrane sample was embedded in a
175 polymeric resin and cut with an ultramicrotome to the required size.
176 *Differential scanning calorimetry (DSC).* Differential scanning calorimetry (DSC) was
177 conducted on a ca. 10 mg sample using a Mettler Toledo DSC822e system. The T_g
178 routine was performed in two cycles from room temperature up to 450 °C at the
179 temperature ramping of 20 °C·min^{-1}. The T_g determination was done in triplicate.
180 *Thermo-gravimetric analysis (TGA).* Thermogravimetric analysis (TGA) was performed
181 using a Mettler Toledo TGA/SDTA 851^e. The analysis was carried out by placing the
182 sample (approximately 10 mg) in an alumina crucible and heating the samples up to 750
183 °C at a ramp of 10 °C·min^{-1} under air flow of 40 mL(STP)·min^{-1}.
184 *X-ray diffraction (XRD).* X-ray diffraction (XRD) patterns of the GO and membranes were
185 obtained by using a Pananalytical Empyrean multipurpose diffractometer (40 kV, 20 mA)
186 with a Cu-Kα (λ = 0.1542 nm) anode, from 2θ of 2.5° to 40° with a 0.03° step·s^{-1}.
187 *Fourier transformed infrared spectroscopy (FTIR)*. FTIR was performed on GO,
188 glutaraldehyde, pristine PVA, cross-linked PVA and the cross-linked PVA-GO 1 wt.%

189 samples, using a Bruker Vertex 70 FTIR spectrometer equipped with a DTGS detector
190 and a Golden Gate diamond ATR accessory. The spectra were recorded in the 4000–
191 600 cm^{-1} wavenumber range at a resolution of 4 cm^{-1}.

192 *Uptake.* The uptake, known as swelling degree, of the cross-linked PVA and MMM
193 membranes was investigated for the 10:90 wt.% water-ethanol mixture following the
194 procedure previously reported by Choi et al. [15]. Three small pieces of membranes (1x5
195 cm) were weighed and immersed in the mixture at 40 ºC for 48 h. The wet membranes
196 were quickly wiped with tissue paper to remove the excess of free liquid on their surface
197 and weighed with a digital balance (Kern, ABJ220-4NM, Germany) with an accuracy of
198 0.001 g. The uptake was calculated as follows:

199 $$Uptake(\%) = \frac{W_w - W_d}{W_d} x\,100 \qquad (1)$$

200 where W_w and W_d were the weights of the wet and dry membranes, respectively.

201 *Water contact angle (CA).* The water contact angle measurements were performed using
202 ultrapure water by the method of the sessile drop using the Krüss DSA 10 MK2
203 instrument. The average and standard deviation values were determined for three
204 measurements.

205 *Mechanical properties.* Mechanical properties of pristine cross-linked PVA membranes
206 and PVA MMMs were determined using a Zwick/Roell Z2.5 test unit (BTC-FR2.5TN-D09,
207 Germany). Measurements were carried out at room temperature (25 °C) using a
208 membrane sample of 1x5 cm. The samples were extended at the constant elongation
209 rate of 5 $mm \cdot min^{-1}$ until their break. Elongation at break, Young's modulus and tensile
210 strength were therefore determined. For each membrane, at least four samples were

211 analyzed and the average and standard deviation were calculated. Mechanical tests were
212 carried out on all the investigated membranes before and after soaking them in a water-
213 ethanol solution (10:90 wt.%) at 25 ºC for 24 h.
214
215 **2.3.2. Pervaporation performance**
216 The PV tests were performed in a semi-continuous laboratory-scale setup. A 10:90 wt.%
217 water-ethanol feed solution (1000 mL) was poured in the feed tank. The operating
218 temperature (at 40, 50, 60 and 70 ºC) was controlled with an accuracy of 0.01 ºC using a
219 thermometer, which was placed inside the membrane cell (in contact with the azeotropic
220 mixture). The vacuum on permeate side was set at 3-4 mbar using a RV3 two-stage
221 vacuum pump (Edwards, UK).
222 The membranes, with an area of 11.7 cm^2, were located on a porous support within the
223 membrane cell. The permeated vapor was condensed and collected in a glass trap placed
224 in a liquid nitrogen condenser. Up to reach the steady-state, the permeates were collected
225 for 8 h and weighted to calculate the total permeate flux (J) as follows:

226 $$J = \frac{Q}{A \times t} \qquad (2)$$

227 where *Q* is the weight of the permeate (kg), *A* is the membrane area (m^2) and *t* is the
228 operating time (h). The partial flux (J_i) for component *i* was determined by multiplying its
229 weight fraction (y_i) in the collected permeate by the total permeate flux (*J*), as Eq. (3)
230 describes:

231 $$J_i = y_i \times J \qquad (3)$$

232 The separation factor (α) was calculated according to Eq. 4:

$$\alpha = \frac{y_{water} / y_{ethanol}}{x_{water} / x_{ethanol}} \qquad (4)$$

where y and x are the weight fractions of the components in the permeate and feed, respectively. The permeate samples were weighed to determine the membrane flux and analyzed with a gas chromatograph (Agilent Technologies, 7820A) equipped with a PORAPAK Q80/100 column using TCD and FID detectors. The J and α values are the averages of more than two runs of 8 h to ensure the accuracy of the results. Every membrane sample was analysed twice which means that the membrane tested as a function of temperature was stable for at least ca. 60 h.

Pervaporation separation factor (PSI) was also calculated as the separation ability of the membranes. PSI is typically expressed as a product of total permeate flux and separation factor, as Eq. (5) describes:

$$PSI = J \cdot \alpha \qquad (5)$$

3. Results and discussion

3.1. Membrane characterization

The glass transition temperature (T_g) for cross-linked PVA membranes was around 95.6±2.8 ºC, as it is displayed in **Table 1**. This value is included in the range (69-110 ºC) that was reported by previous studies [7,15,22]. Furthermore, the MMMs exhibited higher T_g values (around 104-110 ºC) than the pristine PVA membranes. It is well documented that the incorporation of inorganic fillers into a polymer may cause an increase in T_g if there are strong attractive forces between the filler surface and the polymer. Particularly, this change could be attributed to the hydrogen bonding among multiple oxygen

containing functional groups of the GO sheets and the PVA chains rich in alcohol groups [22]. **Figure S1** (supplementary material) shows the TGA curves that can be related to the thermal degradation and stability of the GO and the cross-linked PVA-GO membranes. The first weight loss visible in GO sheets start around 55 °C. Such degradation is attributed to the loss of the water molecules that were retained in its structure and it accounts for 17.7% by weight of the total sample that was analyzed. The second weight loss took place at 200 ºC, and was presumably due to pyrolysis of the labile oxygen-containing functional groups yielding CO, CO_2 and steam [23]. Moreover, it is quite possible that the weight loss may come from the combustion of carbon. Therefore, the decomposition of GO can be accompanied by a vigorous expansion of the gas resulting from the rapid thermal expansion of the material [24] in agreement with the abrupt step observed. This weight loss corresponds to 72.4% by weight of the total material. The last weight loss took place at 550 ºC and it is due to the combustion process. As observed, once dehydrated at ca. 100 ºC, the pristine cross-linked PVA membrane has its degradation step between 300-510 ºC, which corresponds to the complete decomposition of the PVA (weight loss around 85%). Similarly, its MMM-GO membranes presented a first gradual weight-loss (15-19%) starting at 55 ºC, which is more remarkable at the high GO loading. This is probably attributed to the loss of the guest water molecules that could be retained in the GO structure, e.g. water molecules trapped in graphitic domains of GO [25], as well as the water retained in the possible interfacial voids between the GO and PVA matrix. Moreover, there was a weight-loss (between 175-275 ºC) for the MMMs, which was more pronounced as the filler loading increased. This can be related

277 to the GO decomposition. Moreover, the MMMs also presented their degradation step
278 starting at 300 ºC up to 500 ºC. This represents a weight-loss of about 80-85%.
279
280 **Table 1**. T_g and contact angle (CA) values of the pure cross-linked PVA membranes and
281 its MMMs-GO.
282
283 **Figure 2** shows the surface and cross-section FESEM images of the membranes. In case
284 of a surface view, the pure cross-linked PVA membrane (see **Figure 2a**) showed a
285 uniform and smooth surface characteristic without signs of plastic deformation, which is
286 common for cross-linked PVA dense membranes [26]. Whereas the MMMs-GO
287 containing 1 and 2 wt.% slightly lost the uniform surface by increasing the GO content
288 (see **Figure 2c&e**), which could be attributable to the exposure of GO flakes on
289 membrane surface.
290 In cross-sectional view, pure cross-linked PVA membrane presents a typical crater-like
291 pattern which has been already reported by Amirilargani and Sadatnia (2014). Typically,
292 this crater-like pattern is generated during deformation by the freeze fracture of polymeric
293 membranes [27]. Moreover, this pure PVA membrane exhibits a skin layer, or better-
294 known as “top layer”, of about 2.6 μm in thickness. This dense surface layer commonly
295 appears by an extremely short-term reduction of solvent concentration on the surface
296 contacting the air. Such layer tended to be dissipated by incorporating the GO in MMMs.
297 The cross-sectional view also displayed an increase in roughness with an increment in
298 GO loading. When GO concentration reached 2 wt.% the structure showed a tendency of
299 assembling to the membrane surface (see **Figure 2f**), similar to a segregation

phenomenon which has been reported during the GO embedding into chitosan [28]. In fact, in case of cross-linked PVA- GO 2 wt.% membrane, **Figure S2** shows the XRD patterns obtained from its top (with the mentioned skin layer) and bottom layers of the dense membrane, where it can be seen that the presence of GO shifted slightly the PVA signal. This, more evident at the highest GO loading, is in agreement with the floating suffered by the GO sheets during MMM preparation that tend to be accumulated on the top of the MMM. Furthermore, the GO seems to be parallelly deposited to the membrane surface, this pattern has been observed when embedding into polyimide [29] and PVDF [30]. This particular orientation can be related to the remaining functional groups on the edges of GO on every side. Therefore, it is quite probable that GO sheets would have this preferred alignment over the membrane [22,30].

Figure 2. Surface and cross-section FESEM images of pure cross-linked PVA (a, b) and MMMs at 1 wt.% (c, d) and 2 wt.% (e, f) GO content, respectively.

The morphology of GO flakes was investigated by TEM. **Figure 3a** shows a single GO flake with sheet-like multilayer structure, typical for GO, with approximately 200 nm in diameter and evident high aspect ratio. GO sheets are regularly distributed in cross-linked PVA-GO 1 wt.% membrane (see **Figure 3b**) that is in agreement with the homogeneous color of the membrane shown in **Figure 1**. **Figure 3c** presents TEM images of GO sheets in cross-linked PVA-GO 1 wt.% membrane with an angle of observation of -26º, 0º and 27º, respectively. The target of measuring at different angles was to confirm that the material possesses high aspect ratio and sheet-like multilayer structure. This is not so

evident in the dark GO agglomerates of **Figure 3c**. However, near such GO agglomerates thin GO flakes are envisaged, and their form changes with the angle producing “shadows” of different shape, size and greyscale due to their different alignment to the electron beam. This is usually considered as a proof of lamellar nature of the filler in these kind of membranes [31,32].

Continuing with the TEM observation, as can be seen in the inset of **Figure 3d** the electron diffraction pattern of particles embedded in the membrane corresponds to an ordered material with three reticular planes parallel to the electron beam. In fact, six spots can be observed in the reciprocal space that correspond to planes (1 0 0), (1 -1 0) and (0 1 0) of graphene oxide. The d-spacings of such planes have been measured, resulting in a mean value of 0.20 ± 0.01 nm. The side of the hexagons is ca. 0.12 nm, which is consistent with the length of the covalent bonds between carbon atoms in graphene oxide [33]. The inset of **Figure 3e** shows a GO flake in the MMM and its reciprocal space (inset). Two spots can be observed that correspond to planes (0 0 2), with a d-spacing equal to 0.38 ± 0.00 nm. Moreover, the d-spacing between (0 0 1) reticular planes is 0.76 nm, similar to that reported by Strankowski et al. [34]. Finally, in the images of the Fourier transform (insets of Figure 3d and 3e), the bright circles are due to a destructive interference of diffracted electrons, indicating the presence of an amorphous material, in this case the PVA matrix.

Figure 3. TEM images of GO flakes (a), distribution of GO flakes in MMM (b), GO flake in MMM observed at different angles -26º, 0º and 27º (c), GO flakes in MMM and Fourier transform of the selected zone.

The X-ray diffractogram of the GO exhibited a sharp diffraction peak at $2 \cdot \theta = 11.8^{\circ}$ corresponding to d-spacing of 0.75 nm, that agrees with the reported values [35] (see **Figure 4**). Furthermore, this value is in good agreement with that calculated by TEM. The shift of the GO peak position from its primary material (graphite) is due to the presence of oxygen-containing functional groups that intercalate into the space between individual graphene sheets provoking an increase of the d-spacing [36]. Moreover, the pure PVA displays a strong diffraction peak at $2 \cdot \theta = 19.6^{\circ}$, which was less intense after the cross-linking procedure. Furthermore, some peaks at 12º and 22º in PVA were identified. These peaks disappeared later, what is normally attributed to the reduction of crystallinity of PVA membranes by the cross-linking [7]. The cross-linked PVA-GO MMMs also exhibited similar features with a slight change compared to the pure one. No peak corresponding to GO sheets was discernible, which can be due to the low loading of the material in the MMMs, in agreement with analogous GO-PVA reinforced composites [22]. Moreover, the absence of diffraction peaks related to the GO interlayer spacing may also be due to the lack of preferential orientation of the GO flakes [37]. However, the GO loading could be enough to modify the spacing of polymer chains [7].

Figure 4. XRD patterns of the pure PVA, pure GO, cross-linked PVA and its MMMs-GO.

Regarding the FTIR spectra, **Figure 5** exhibits standard absorption peaks for the PVA polymer. The presence of characteristic absorption peaks at ~1100 cm^{-1} and ~1150 cm^{-1} can be seen. A modest change was noticed a distinct and broad -OH stretch at ~3200

369 cm^{-1} that appeared due to the cross-linking procedure using glutaraldehyde. Such change
370 can be attributed to the presence of alcohols for intermolecular hydrogen bonds in the
371 polymer. Moreover, as reported by Kashyap et al. [22], the PVA-GO MMMs exhibited
372 similar features with a slight shift of the peak to lower wavenumbers, displaying strong
373 interfacial interactions between the polymer matrix and GO.
374
375 **Figure 5.** FTIR spectroscopy of the GO, glutaraldehyde, pristine PVA, cross-linked PVA
376 and the PVA-GO 1 wt.% samples.
377
378 The measured water contact angle value for cross-linked PVA membrane was around
379 69.6º±0.5º, as it is reported in **Table 1**. The obtained value which is within the range of
380 57º-77º is in agreement with that reported by several authors [26,38]. The hydrophilicity
381 depends on the type of cross-linker used and the consumption of –OH groups during the
382 cross-linking [26,38]. However, the hydrophilic nature was still confirmed in the cross-
383 linked membranes. On the other hand, the cross-linked PVA displayed an enhanced
384 hydrophilicity by embedding GO into its matrix, e.g. up to 58.4º±0.5º for the MMMs-GO 2
385 wt.%. Generally, the water contact angle decreased with an increase of GO content. This
386 is related to the abundant oxygen-containing functional groups on the wrinkled GO sheets
387 [28]. In addition, the enhancement of water contact angle of MMMs was leveled off when
388 GO content was higher than 1 wt.%, whereas it did not show strong change in case of 2
389 wt.%. GO caused a decrease of water contact angle also in other MMMs based on
390 chitosan [28,39] and polyimides [40]. In theory, the wettability of a membrane is directly
391 associated with the water adsorption rate on the membrane surface, which is highly

important in PV since it is considered as the first step of water transport through the membrane based on the solution-diffusion mass transfer mechanism.

The uptake of membranes was carried out from their contact with 10/90 wt.% water-ethanol solution (the same concentration used in the PV experiments). The calculated uptake results are depicted in **Figure 6.** It can be seen that the uptake decreased with an increase of the GO content. This tendency has been reported during the incorporation of GO into hydrophilic chitosan membranes [28]. Basically, the decrease in uptake is related to the strong GO-polymer interactions which, besides reducing the availability of hydrophilic groups, could restrict the mobility of PVA chains and decrease even more the free volume of the cross-linked PVA. GO has demonstrated, as multi-walled carbon nanotubes [15], to suppress the swelling degree of these PVA membranes. Therefore, GO provides better stability in the cross-linked PVA against the swelling phenomenon. Finally, it is worth to mention that the cross-linking made the membrane more resistant to the ethanol-water mixture that would otherwise dissolve.

Figure 6. Uptake of the cross-linked PVA and MMMs-GO membranes at 10:90 wt.% water-ethanol (at 40 ºC).

As can be seen from **Figure 7**, the addition of GO has a relevant effect on the mechanical properties of the pristine cross-linked PVA membranes. The incorporation of GO led to a general improvement of the mechanical behavior of the pristine membranes in terms of Young's modulus, tensile strength and elongation at break. The tensile strength value, for instance, displayed in **Figure 7c**, increased from 27 $N \cdot mm^{-2}$ for the pristine PVA

membrane up to 43 $N \cdot mm^{-2}$ for the membrane loaded with 0.5 wt.% GO with an increase of tensile strength of about 60%. The increase was particularly pronounced for lower GO loadings (0.5 and 1 wt.%). An improvement of Young's modulus was also observed for all the MMMs by adding GO (**Figure 7a**) in particular at the lowest filler content, e.g. a 134% increase was observed in comparison to the pristine one. The elongation at break, after an initial increase at 0.5 wt.% GO (from 103% to 154 %) tended to decrease at the highest GO concentration (down to 32%) (**Figure 7b**). This could be due to the interaction of GO with the membrane matrix that hinders the movement of the polymer chains at high filler concentrations [41], in line with the above discussed increases of T_g values (See **Table 1**). This trend of the change of mechanical properties is similar to that observed by Zhao et al. [41], where PVA membranes were loaded with different concentrations of graphene nanosheets. They observed an increase in the tensile strength from 17 $N \cdot mm^{-2}$ for the pristine PVA membrane to 42 $N \cdot mm^{-2}$ for the membranes loaded with 1.8 vol% of graphene nanosheets. The Young's modulus also increased from 1000 $N \cdot mm^{-2}$ to about 10000 $N \cdot mm^{-2}$ when graphene (1.8 vol%) was added to the PVA. The authors explained these results stating that there exists a critical point of graphene nanosheets loading (called mechanical percolation) [22], where beyond this concentration there is no improvement in the membrane mechanical properties due to the stacking of nanosheets. Hence, by diminishing this concentration (which they found at 1.8 vol% for graphene sheets), an improvement in the membrane mechanical properties can be obtained due to the better dispersion of the filler in the polymer matrix. In this work, the critical point can be identified at the 1 wt.% GO content. As can be observed in **Figure 7a&c**, the membrane mechanical properties were greatly improved below this value. A similar trend

438 was also observed and reported by Kashyap et al. [22] during the reinforcement of PVA
439 polymer matrices, where at low GO concentrations (0.3 wt.% only) the mechanical
440 properties of PVA membranes were enhanced. This improvement was attributed to the
441 uniform dispersion of the GO in the membrane and to the strong hydrogen bonding
442 interfacial interaction between the filler and membrane matrix.
443
444 **Figure 7**. Mechanical properties of cross-linked PVA membrane and MMMs-GO before
445 and after exposure to water-ethanol (10:90 wt.%) mixture.
446
447 Moreover, the mechanical properties were also measured for the pristine PVA membrane
448 and its MMMs after soaking them in a water-ethanol solution (10:90 wt.%) during 24 h. A
449 general decrease of the mechanical properties in terms of Young's modulus and tensile
450 strength was observed after exposure of the membranes to the solution. The mechanical
451 properties of the membranes, therefore, may be subjected to a plasticization effect due
452 to the hydrogen bonds formation between polar molecules (i.e. from ethanol and water)
453 and PVA polymer. As a consequence, in the swollen state, the chain-chain polymer
454 interactions decreased resulting in a contraction of the membranes. Commonly, the
455 exposure to the water-ethanol solution led to a swelling phenomenon in membranes of
456 poly(lactic acid)/poly(vinyl pyrrolidone) [42]. On the contrary, the elongation at break of
457 the MMMs containing 0.5 and 1 wt.% GO was slightly enhanced after soaking (**Figure**
458 **7b**).
459
460

3.2. Pervaporation tests

3.2.1. Effect of GO loading and temperature on PV performance

Figure 8 displays the effect on GO content of the total permeate flux during the PV performance as a function of the operating temperature (data available in supplementary material, **Table S1**). Essentially, an increment in the total permeation rate was observed with a double increase of GO loading. This tendency is commonly observed during the incorporation of the inorganic materials into polymer membranes, which may be a result of the free volume increase as well as the possible interfacial selective gaps between GO sheets and PVA matrix, while the highly hydrophilic nature of the filler can also produce a raise in the permeation rates by preferential adsorption of the more polar compound (water). Moreover, an escalation on the total permeation was observed with temperature increase (40-70 ºC). In theory, the polymer chains tend to be more flexible at higher temperatures promoting the sorption ability of the components, leading to the increase of permeating compounds through the intermolecular distances of the polymeric membrane. Also, the viscosity of the liquid feed diminishes with temperature favoring the permeate transport through the membrane.

Figure 8. Total permeate flux as a function of the GO loading at different operating temperatures (10:90 wt.% water-ethanol). The curves are only guides to the eye.

The effect of the temperature on total permeate flux can be analyzed by using the so-called Arrhenius relationship (Eq. 5) [43], as follows:

$$J = J_o \cdot \exp\left(-\frac{E_a}{R \cdot T}\right) \qquad (5)$$

Where J_o is the pre-exponential factor, E_a is the apparent activation energy for permeation (for the overall mixture and each component) and $R \cdot T$ is the common energy term. The linearization of the Eq. (5) through logarithmic laws leads to the plot of **Figure S3**, which displays the total fluxes as a function of the reciprocal of temperature at azeotropic conditions. The figure confirms that an Arrhenius relationship exists between total fluxes and operating temperature. i.e. the total flux tends to raise with an increase of the temperature. Furthermore, the apparent activation energy (E_a), which can be calculated as the slope of the curve (**Figure S3**), and using the Eq. (5), can provide an outlook on the relationship between the total flux and the GO content. From **Table 2**, it can be seen that the E_a values for total flux gradually decrease with an increase of filler loading, e.g. 7.0 kJ/mol in the pristine PVA membranes to 1.9 kJ/mol in the MMMs-2 wt.% GO. At this point, the E_a decrease towards water was more influenced than that for ethanol in the range of handled temperature (40-70°C). Importantly, the PV process in the handled temperature affects mainly the permeation rate of water, and does influence minimally the ethanol permeation. While the presence of GO contributes to the reduction of the energy needed for the components to permeate across the membranes [44]; similar behavior was recently reported by Qian et al. [28] during the PV desalination of water through chitosan-GO membranes.

503 **Table 2**. Apparent activation energies for total permeate, water and ethanol partial fluxes
504 of the PVA membrane and its MMMs at different GO loadings (Data obtained from
505 **Figures S3-S5**).
506
507 Regarding the separation factor (water selectivity), see **Figure 9**, a decrease as a function
508 of the temperature for pure cross-linked PVA membrane as well as its MMMs has been
509 observed. Certainly, the decrease of separation factor in the MMMs might be due to the
510 combined effect of several factors, such as characteristics of GO (e.g. GO structure and
511 the influence of its preparation procedure), polymer properties, the effect of the cross-
512 linking procedure on the adsorption capacity of the polymer, and of course, the operating
513 temperature. In principle, high separation factors and lower permeation rates were
514 obtained at the lowest temperatures for all membranes. Based on the free volume theory,
515 the thermal motion of polymer chains in the amorphous regions results in free volume. As
516 temperature increases, the frequency and amplitude of the chain jumping (i.e. thermal
517 agitation) increase and the resulting free volume becomes larger [45]. Therefore, this
518 thermal motion of the polymeric chains may facilitate the diffusion of larger molecules (like
519 ethanol) through the membrane causing a decrease in separation factor, in agreement
520 with the fact that activation energy values for ethanol are always larger than those of
521 water (see **Table 2**). The absence of negative values for the activation energy data
522 reveals that the permeation of the species presented in these MMMs is less governed by
523 the adsorption [44]; indeed, polymer cross-linking strongly tends to affect the membrane
524 adsorption, e.g. in PVA [46]. Moreover, the diffusion of a binary liquid mixture is typically
525 characterized by self- and cross (coupled) - plasticization of a permeant. At this point,

526 self-plasticization of permeants means that the flux of one component is affected only by
527 its own sorption amount.
528 The effect of crystallinity of the PVA membrane also plays an important role in the
529 transport of species. The crystalline regions act as giant cross-linking regions with respect
530 to chains that are partially embedded in several crystallites. The swelling and diffusion
531 are reduced in comparison to those in the totally amorphous polymer. The restriction of
532 crosslinking regions on segmental mobility makes the diffusion process more difficult and
533 dependent on the shape and size of the molecules [47]. In this way, the crystallinity of the
534 PVA can be strongly affected by the cross-linking procedure, as well as the incorporation
535 of inorganic materials into its matrix [15].
536 It is worth mentioning, as **Figure 9** displays, that the separation factor at any of the
537 temperatures did not follow a continuous decreasing trend. From the strict point of view
538 in case of separation factor values (**Table S2** and **Figure 9**), the first addition of GO (0.5
539 wt.%) was not enough to compensate the distortion in the PVA chains that caused the
540 formation of non- selective pores (but hydrophilic), and it was necessary to double the
541 filler amount (1 wt.%) to compensate in part the loss of selectivity. In other words, at 1
542 wt.% GO, the concentration of sheets in the MMMs is high enough as to exert an
543 additional barrier effect to bulkier ethanol molecules (decreasing the ethanol PV flux
544 through the membrane, see **Figure 10**) and thus to recover part of the separation factor
545 of the bare cross-linked PVA membrane. Nevertheless, the MMMs-2 wt.% GO had an
546 excess of filler and the separation factor worsened in agreement with the loss of
547 mechanical properties seen above.
548

549 **Figure 9**. Separation factor as a function of the GO loading at different operating
550 temperatures (10: 90 wt.% water-ethanol). The lines are only guides to the eye.
551
552 **Figure 10**. Water and ethanol partial fluxes as a function of the GO loading at different
553 operating temperatures (10:90 wt.% water-ethanol). The curves are only guides to the
554 eye.
555
556 Definitely, the modification of PVA with GO filler favors the preferential transport of water.
557 This is due to the fact that GO laminates simultaneously have oxidized (proper GO,
558 hydrophilic) and non-oxidized (graphene, hydrophobic) regions. The non-oxidized regions
559 of graphene sheets possess a d-spacing of ca. 5 Å [48], which is enough to host a
560 monolayer of water (kinetic diameter=2.68 Å). It has been speculated that these empty
561 spaces form a network of pristine-graphene capillaries within GO laminates [49], which
562 would facilitate the water transport. **Figure 11** shows a scheme of the possible water
563 permeation mechanism involving GO species. It has been reported that, even when the
564 mixture of water and other compounds (e.g. gases and liquids) was fed, the water
565 permeation rate was at least five orders of magnitude higher than that of the other
566 components [49,50]. In fact, using equilibrium molecular dynamics simulations, it has
567 been stated that water can easily flow through graphene nano-channels (e.g., the non-
568 oxidized region of GO) [51]. Importantly, taking into account that graphene sheets
569 possess a d-spacing of ca. 5 Å, this d-spacing is still slightly larger than the kinetic
570 diameter of the ethanol molecules (4.5 Å) [15], which may allow them passing through.
571 However, interestingly, this characteristic d-spacing of GO can be enlarged in the

presence of water. For instance, the interlayer spacing can vary from ≈6.4 to 9.8 Å with relative humidity changes from 0 to 100% [37]. Thereby, water and ethanol molecules can surely pass through the channels of GO; however, according to our findings and the ones in literature, GO is still displaying a preferential transport of water [25].

Figure 11. Schematic drawing of the possible water permeation mechanism through GO laminates. Inspired by Nair et al. (2012).

To date, it is clear that the water transport mechanism in the GO laminar structure is still not well understood and established, particularly in pervaporation which involves selective permeation and evaporation [25]. Especially, when using GO membranes, the separation of water from organics is mainly related to preferential adsorption of water in GO [52], such preferential adsorption has been attributed to the large amount of hydrophilic functional groups in GO and the low water condensation partial pressure according to the fine laminar structure. Herein, solution–diffusion (also known as adsorption–diffusion) model has been widely sought to explain such phenomenon. However, while the preferential adsorption of water has been repeatedly confirmed by many researchers, the diffusion of water in GO membranes is not much discussed in terms of adsorption–diffusion model [52,53]. This description addressing the adsorption phenomenon (governed by concentration gradient) compromise the hypothesis provided by Nair et al. [49], in which the explanation about the transport of water in the interlayer space follows a pore flow model (governed by pressure difference). In this sense, Chong et al. [25]

595 analyzed the water transport through GO membranes using two different modes:
596 pressure-driven permeation and pervaporation. Basically, the authors stated that pure
597 water flux is 1–2 orders of magnitude higher in PV due to the large capillary pressure
598 induced by evaporation.
599 Finally, the decrease in separation efficiency can also be affected by the synthesis of GO.
600 According to Hung et al. [53], it is extremely challenging to form highly ordered and
601 precise GO laminates. It has been reported that the repulsive electrostatic interactions
602 produced by negatively charged carboxyl groups might create some out-of-order
603 accumulation (i.e. wrinkles). Also, a large number of nonselective defects (basic plane
604 holes) derived from the strong oxidization conditions applied to obtain GO may penalize
605 the membrane separation performance [50].
606
607 *3.2.2. Comparison of cross-linked PVA-GO MMMs with other studies*
608 The performance of polymeric and MMMs for any water-organic separation, like water-
609 ethanol, through PV, depends directly on: i) the polymer characteristics (e.g. material
610 type, nature, structure, thickness); the filler features (e.g. shape, size,
611 hydrophilicity/hydrophobicity, morphology); iii) the physico-chemical properties and
612 concentration of the compounds in the mixture to be separated; and iv) the operating
613 conditions (e.g. temperature, vacuum pressure, feed flow rate) [54,55]. This makes
614 difficult to fairly compare PV data with works where different conditions have been
615 applied, bearing also in mind that our work is the first one dealing with the use of cross-
616 linked PVA-GO membranes for water-ethanol separation by PV. Having said that, **Table**

3 compares water-ethanol PV performances of a number of MMMs filled with carbonaceous materials, zeolites, MOFs and several porous and non-porous oxides.

Table 3. Comparison of the cross-linked PVA-GO MMMs performance with other studies for the dehydration of ethanol.

It is a challenging task selecting the best performance of cross-linked PVA-GO MMMs obtained in the current work in terms of permeate flux and separation factor, because cross-linked PVA membrane itself possesses high separation efficiencies (α =163-518 with total PV fluxes= 0.079-0.131 $kg \cdot m^{-2} \cdot h^{-1}$, see **Tables S1** and **S2** and **Figures 8** and **9**) depending on handled temperature. Considering the MMMs containing 1 wt.% GO as the optimum loading (α=88.2-263 with total PV fluxes=0.137-0.162 $kg \cdot m^{-2} \cdot h^{-1}$, see **Tables S1** and **S2** and **Figures 8** and **9**), their separation factors are higher than those of other membranes based on chitosan-H-ZSM-5 [13], chitosan-TiO_2 [56], cross-linked PVA-ZIF-8-NH_2 [16] and polyimide-MSS-1 [6]; but lower than those corresponding to membranes of cross-linked sodium alginate-beta zeolite [11], polyimide-ZIF-8 [6], cross-linked sodium alginate-zeolite [57], PVA-MWCNT [15], and cross-linked chitosan-silica [58].

Moreover, the pristine cross-linked PVA displays relatively acceptable total permeate flux (J=0.079-0.131 $kg \cdot m^{-2} \cdot h^{-1}$), while its MMMs containing 2 wt.% GO have shown the highest permeate flux values of about 0.185 $kg \cdot m^{-2} \cdot h^{-1}$ (at 70 ºC). Such fluxes are higher than the reported ones using cross-linked sodium alginate-beta zeolite [11], PVA-MWCNT [15], and cross-linked sodium alginate-zeolite [57]; however, other MMMs provided even higher permeation fluxes than the ones presented in this study, such as chitosan-H-ZSM-

5 [13], polyimide-ZIF-8 [6], chitosan- TiO_2 [56], polyimide-MSS-1 [6] and cross-linked chitosan-silica [58]. It is important to highlight that the current PV flux enhancements obtained with the cross-linked PVA-GO MMMs that enlarge permeate flux (mainly towards water) were obtained by incorporating a small amount of GO filler, which is much lower compared to previous studies. Finally, regardless of the amount of GO used for the preparation of these membranes, the right choice of the MMM will depend on the final purpose (high productivity or high separation efficiency), as well as the feasibility of the process considering primordially its operating conditions, e.g. temperature, that indeed influences on the PV performance.

When dealing with the separation performance of PV membranes, it is useful to compare their separation ability by means of PSI (see **Table 3**). It can be seen that the PVA-GO MMMs (1 wt.%) display better PSI values in comparison to some MMMs based on chitosan-H-ZSM-5, cross-linked PVA-ZIF-8-NH_2, and some commercial membranes (PVA composites). However, there are still some other membranes that present superior performances, such as cross-linked sodium alginate-zeolite beta, chitosan-TiO_2, polyimide-MSS-1, cross-linked chitosan-silica and polyimide-ZIF-8. Finally, permeance and selectivity are the best way of reporting pervaporation results when a fair comparison of different studies is needed (considering experiments at different feed concentrations, feed temperatures and permeate pressures) [55]. Permeance should be independent on the driving force and should just describe the system membrane/permeating component. In this way, the PV data for all MMMs are also provided for the readers (data available in supplementary material; **Table S5**).

4. Conclusions

Cross-linked-PVA membranes containing GO have been successfully tested for the PV separation of the water-ethanol azeotropic mixture. The effect of operating temperature has been evaluated. The best performance of cross-linked PVA-GO membranes has been provided by the one containing 1 wt.% filler, displaying an acceptable separation factor (263, at 40 ºC) with a high permeate total flux of about 0.137 $kg \cdot m^{-2} \cdot h^{-1}$ (in which 0.133 $kg \cdot m^{-2} \cdot h^{-1}$ corresponds to water). At this point, these MMMs, having only 1 wt.% GO, have demonstrated the enhancement of the permeation performance of pristine cross-linked PVA membranes, by over 75 % compared to their original permeation rates. Of course, higher permeate fluxes can be obtained by increasing *i)* the temperature, since the total, water and ethanol fluxes have shown a positive temperature dependence; and *ii)* filler loading, e.g. 2 wt.% GO. Based on the obtained results, it is possible to conclude that these PVA MMMs membranes have a promising potential to be used in PV for the dehydration of ethanol. Moreover, regarding the use of these MMMs in a “green” process, the incorporation of GO has satisfactorily enhanced the water transport of cross-linked PVA membranes, displaying losses on selectivity. However, the high water permeation fluxes could contribute to use less energy-requirement due to the less operating time may be needed to reach pure ethanol.

Finally, MMMs containing 1 wt.% GO have been considered as the optimum membranes with a good PV flux-separation factor ratio. This is in good agreement with better thermal (T_g) and mechanical properties (Young’ modulus, elongation at break and tensile strength) exhibited by these MMMs in comparison to those at 0.5 and 1 wt.% GO loading.

Associated content

TGA curves of the cross-linked PVA membranes and its MMMs. XRD patterns of the cross-linked PVA-GO 2 wt.% membrane (top and bottom layer) and GO. Pervaporation data (total flux, water flux, ethanol flux, separation factor, water permeance, ethanol permeance, and selectivity) as a function of the GO loading at different operating temperatures. Temperature dependence curves of total permeate, water and ethanol flux by Arrhenius plot at different GO loadings.

Acknowledgments

R. Castro-Muñoz acknowledges the European Commission - Education, Audiovisual and Culture Executive Agency (EACEA) for his PhD scholarship under the program: Erasmus Mundus Doctorate in Membrane Engineering – EUDIME (FPA No 2011-0014, Edition V, http:/eudime.unical.it). This work was partially supported by the Operational Program Prague – Competitiveness (CZ.2.16/3.1.00/24501) and the “National Program of Sustainability“ (NPU I LO1613) MSMT-43760/2015. Financial support from the Spanish MINECO and FEDER (MAT2016-77290-R), the Aragón Government (T43-17R) and the ESF is also gratefully acknowledged.

Note

The authors declare no conflict of interest.

References

[1] P. Luis, B. Van Der Bruggen, The driving force as key element to evaluate the

709 pervaporation performance of multicomponent mixtures, Sep. Purif. Technol. 148
710 (2015) 94–102.
711 [2] J. Crespo, C. Brazinha, Fundamentals of pervaporation, in: A. Basile, A. Figoli, M.
712 Khayet (Eds.), Pervaporation, Vap. Permeat. Membr. Distill., Elsevier Ltd.,
713 Cambridge UK, 2015: pp. 1–17.
714 [3] P.T. Anastas, J.C. Warner, Green Chemistry: Theory and Practice, Oxford
715 University Press, New York, 1998.
716 [4] Y.K. Ong, G.M. Shi, N.L. Le, Y.P. Tang, J. Zuo, S.P. Nunes, T.S. Chung, Recent
717 membrane development for pervaporation processes, Prog. Polym. Sci. 57 (2016)
718 1–31.
719 [5] R. Castro-Muñoz, F. Galiano, V. Fíla, E. Drioli, A. Figoli, Mixed matrix membranes
720 (MMMs) for ethanol purification through pervaporation : current state of the art,
721 Rev. Chem. Eng. https//doi.org/10.1515/revce-2017-0115. (2018).
722 [6] A. Kudasheva, S. Sorribas, B. Zornoza, C. Téllez, J. Coronas, Pervaporation of
723 water/ethanol mixtures through polyimide based mixed matrix membranes
724 containing ZIF-8, ordered mesoporous silica and ZIF-8-silica core-shell spheres,
725 J. Chem. Technol. Biotechnol. 90 (2015) 669–677.
726 [7] M. Amirilargani, B. Sadatnia, Poly (vinyl alcohol)/ zeolitic imidazolate frameworks
727 (ZIF-8) mixed matrix membranes for pervaporation dehydration of isopropanol,
728 J. Memb. Sci. 469 (2014) 1–10.
729 [8] V. Van Hoof, C. Dotremont, A. Buekenhoudt, Performance of Mitsui NaA type
730 zeolite membranes for the dehydration of organic solvents in comparison with
731 commercial polymeric pervaporation membranes, Sep. Purif. Technol. 48 (2006)

304–309.

[9] RFA, World Fuel Ethanol Production, Renew. Fuels Assoc. (2017). http://www.ethanolrfa.org/resources/industry/statistics/#1454098996479-8715d404-e546 (accessed January 22, 2018).

[10] J.-H. Chang, J.-K. Yoo, S.-H. Ahn, K.-H. Lee, S.-M. Ko, Simulation of pervaporation process for ethanol dehydration by using pilot test results, Korean J. Chem. Eng. 15 (1998) 28–36.

[11] S.G. Adoor, L.S. Manjeshwar, S.D. Bhat, T.M. Aminabhavi, Aluminum-rich zeolite beta incorporated sodium alginate mixed matrix membranes for pervaporation dehydration and esterification of ethanol and acetic acid, J. Memb. Sci. 318 (2008) 233–246.

[12] G.M. Shi, T. Yang, T.S. Chung, Polybenzimidazole (PBI)/zeolitic imidazolate frameworks (ZIF-8) mixed matrix membranes for pervaporation dehydration of alcohols, J. Memb. Sci. 415–416 (2012) 577–586.

[13] H. Sun, L. Lu, X. Chen, Z. Jiang, Pervaporation dehydration of aqueous ethanol solution using H-ZSM-5 filled chitosan membranes, Sep. Purif. Technol. 58 (2008) 429–436.

[14] E. Okumuş, T. Gürkan, L. Yilmaz, Effect of fabrication and process parameters on the morphology and performance of a PAN-based zeolite-filled pervaporation membrane, J. Memb. Sci. 223 (2003) 23–38.

[15] J.H. Choi, J. Jegal, W.N. Kim, H.S. Choi, Incorporation of Multiwalled Carbon Nanotubes into Poly(vinyl alcohol) Membranes for Use in the Pervaporation of Water/Ethanol Mixtures, J. Appl. Polym. Sci. 111 (2008) 2186–2193.

[16] Y. Zhang, H., Wang, Poly(vinyl alcohol)/ZIF-8 NH2 Mixed Matrix Membranes for Ethanol Dehydration via Pervaporation, AIChE J. 62 (2016) 1728–1739.

[17] V. Singh, D. Joung, L. Zhai, S. Das, S.I. Khondaker, S. Seal, Graphene based materials: Past, present and future, Prog. Mater. Sci. 56 (2011) 1178–1271.

[18] H.K. Dave, K. Nath, Graphene oxide incorporated novel polyvinyl alcohol composite membrane for pervaporative recovery of acetic acid from vinegar wastewater, J. Water Process Eng. 14 (2016) 124–134.

[19] N. Wang, S. Ji, J. Li, R. Zhang, G. Zhang, Poly(vinyl alcohol)-graphene oxide nanohybrid “pore-filling” membrane for pervaporation of toluene/n-heptane mixtures, J. Memb. Sci. 455 (2014) 113–120.

[20] S. Castarlenas, C. Téllez, J. Coronas, Gas separation with mixed matrix membranes obtained from MOF UiO-66-graphite oxide hybrids, J. Memb. Sci. 526 (2017) 205–211.

[21] W.S. Hummers, R.E. Offeman, Preparation of Graphitic Oxide, J. Am. Chem. Soc. 80 (1958) 1339.

[22] S. Kashyap, S.K. Pratihar, S.K. Behera, Strong and ductile graphene oxide reinforced PVA nanocomposites, J. Alloys Compd. 684 (2016) 254–260.

[23] G. Wang, Z. Yang, X. Li, C. Li, Synthesis of poly(aniline-co-o-anisidine)-intercalated graphite oxide composite by delamination/reassembling method, Carbon N. Y. 43 (2005) 2564–2570.

[24] S. Stankovich, D.A. Dikin, R.D. Piner, K.A. Kohlhaas, A. Kleinhammes, Y. Jia, Y. Wu, S.B.T. Nguyen, R.S. Ruoff, Synthesis of graphene-based nanosheets via chemical reduction of exfoliated graphite oxide, Carbon N. Y. 45 (2007) 1558–

778 1565.
779 [25] J.Y. Chong, B. Wang, K. Li, Water transport through graphene oxide membranes :
780 the roles of driving forces, Chem. Commun. 54 (2018) 2554–2557.
781 [26] R. Zhang, X. Xu, B. Cao, P. Li, Fabrication of high-performance PVA / PAN
782 composite pervaporation membranes crosslinked by PMDA for wastewater
783 desalination, Pet. Sci. 15 (2018) 146–156.
784 [27] F. Dorosti, M. Omidkhah, R. Abedini, Fabrication and characterization of
785 Matrimid/MIL-53 mixed matrix membrane for CO2/CH4 separation, Chem. Eng.
786 Res. Des. 92 (2014) 2439–2448.
787 [28] X. Qian, N. Li, Q. Wang, S. Ji, Chitosan/graphene oxide mixed matrix membrane
788 with enhanced water permeability for high-salinity water desalination by
789 pervaporation, Desalination. 438 (2018) 83–96.
790 [29] X. Li, L. Ma, H. Zhang, S. Wang, Z. Jiang, R. Guo, H. Wu, X.Z. Cao, J. Yang, B.
791 Wang, Synergistic effect of combining carbon nanotubes and graphene oxide in
792 mixed matrix membranes for efficient CO2separation, J. Memb. Sci. 479 (2015)
793 1–10.
794 [30] E.A. Feijani, A. Tavassoli, H. Mahdavi, H. Molavi, Effective gas separation
795 through graphene oxide containing mixed matrix membranes, J. Appl. Polym. Sci.
796 135 (2018) 1–11.
797 [31] C. Rubio, C. Casado, P. Gorgojo, F. Etayo, S. Uriel, C. Téllez, J. Coronas,
798 Exfoliated Titanosilicate Material UZAR-S1 Obtained from JDF-L1, Eur. J. Inorg.
799 Chem. 1 (2010) 159–163.
800 [32] S. Choi, J. Coronas, E. Jordan, W. Oh, S. Nair, F. Onorato, D.F. Shantz, M.

Tsapatsis, Layered Silicates by Swelling of AMH-3 and Nanocomposite Membranes **, Angew. Chem. Int. Ed. 47 (2008) 552–555.

[33] N.R. Wilson, P.A. Pandey, R. Beanland, R.J. Young, I.A. Kinloch, L. Gong, Z. Liu, Ќ.K. Suenaga, Ќ.J.P. Rourke, S.J. York, J. Sloan, Graphene Oxide : Structural Analysis and Application as a Highly Transparent Support for Electron Microscopy, ACS Nano. 3 (2009) 2547–2556.

[34] M.B. Strankowski, W.B. Damian, A. Piszczyk, J. Strankowska, Polyurethane Nanocomposites Containing Reduced Graphene Oxide, FTIR, Raman, and XRD Studies, J. Spectrosc. 2016 (2016) 1–6.

[35] K. Krishnamoorthy, M. Veerapandian, K. Yun, S.J. Kim, The chemical and structural analysis of graphene oxide with different degrees of oxidation, Carbon N. Y. 53 (2013) 38–49.

[36] D.R. Dreyer, S. Park, C.W. Bielawski, R.S. Ruoff, The chemistry of Graphite oxide, Chem. Soc. Rev. 39 (2010) 228–240.

[37] J. Abraham, K.S. Vasu, C.D. Williams, K. Gopinadhan, Y. Su, C.T. Cherian, J. Dix, E. Prestat, S.J. Haigh, I. V Grigorieva, P. Carbone, A.K. Geim, R.R. Nair, Tunable sieving of ions using graphene oxide membranes, Nat. Nanotechnol. (2017) 1–6.

[38] R. Zhang, B. Liang, T. Qu, B. Cao, P. Li, High-performance sulfosuccinic acid cross-linked PVA composite pervaporation membrane for desalination, Environ. Technol. (United Kingdom). 3330 (2017) 1–9.

[39] S.P. Dharupaneedi, R. V. Anjanapura, J.M. Han, T.M. Aminabhavi, Functionalized graphene sheets embedded in chitosan nanocomposite membranes for ethanol

824 and isopropanol dehydration via pervaporation, Ind. Eng. Chem. Res. 53 (2014)
825 14474–14484.
826 [40] B. Feng, K. Xu, A. Huang, Synthesis of graphene oxide/polyimide mixed matrix
827 membranes for desalination, RSC Adv. 7 (2017) 2211–2217.
828 [41] X. Zhao, O. Zhang, D. Chen, Enhanced Mechanical Properties of Graphene-
829 Based Poly(vinyl alcohol) Composites, Macromolecules. 43 (2010) 2357–2363.
830 [42] S. Zereshki, A. Figoli, S.S. Madaeni, S. Simone, J.C. Jansen, M. Esmailinezhad,
831 E. Drioli, Poly(lactic acid)/poly(vinyl pyrrolidone) blend membranes: Effect of
832 membrane composition on pervaporation separation of ethanol/cyclohexane
833 mixture, J. Memb. Sci. 362 (2010) 105–112.
834 [43] R. Castro-Muñoz, F. Galiano, V. Fíla, E. Drioli, A. Figoli, Matrimid®5218 dense
835 membrane for the separation of azeotropic MeOH-MTBE mixtures by
836 pervaporation, Sep. Purif. Technol. 199 (2018) 27–36.
837 [44] D.S.M. Constantino, R.P.V. Faria, A.M. Ribeiro, J.M. Loureiro, A.E. Rodrigues,
838 Performance Evaluation of Pervaporation Technology for Process Intensification
839 of Butyl Acrylate Synthesis, Ind. Eng. Chem. Res. 56 (2017) 13064–13074.
840 [45] R. Huang, C. Yeom, Pervaporation separation of aqueous mixtures using
841 crosslinked poly(vinyl alcohol)(pva). II. Permeation of ethanol-water mixtures, J.
842 Memb. Sci. 51 (1990) 273–292.
843 [46] T.F. Ceia, A.G. Silva, C.S. Ribeiro, J. V. Pinto, M.H. Casimiro, A.M. Ramos, J.
844 Vital, PVA composite catalytic membranes for hyacinth flavour synthesis in a
845 pervaporation membrane reactor, Catal. Today. 236 (2014) 98–107.
846 [47] C.H. Lee, W.H. Hong, Influence of different degrees of hydrolysis of poly (vinyl

847 alcohol) membrane on transport properties in pervaporation of IPA / water
848 mixture, J. Memb. Sci. 135 (1997) 187–193.
849 [48] S. Homaeigohar, M. Elbahri, Graphene membranes for water desalination, NPG
850 Asia Mater. 9 (2017) e427.
851 [49] R.R. Nair, H.A. Wu, P.N. Jayaram, I.V. Grigorieva, A.K. Geim, Unimpeded
852 Permeation of Water Through Helium-Leak–Tight Graphene-Based Membranes,
853 Science (80-.). 335 (2012) 442–445.
854 [50] K. Huang, G. Liu, W. Jin, Vapor transport in graphene oxide laminates and their
855 application in pervaporation, Curr. Opin. Chem. Eng. 16 (2017) 56–64.
856 [51] S. Kumar Kannam, B.D. Todd, J.S. Hansen, P.J. Daivis, Slip length of water on
857 graphene: Limitations of non-equilibrium molecular dynamics simulations, J.
858 Chem. Phys. 136 (2012).
859 [52] K. Huang, G. Liu, Y. Lou, Z. Dong, J. Shen, W. Jin, A Graphene Oxide Membrane
860 with Highly Selective Molecular Separation of Aqueous Organic Solution, Angew.
861 Chemie - Int. Ed. 53 (2014) 6929–6932.
862 [53] W.S. Hung, Q.F. An, M. De Guzman, H.Y. Lin, S.H. Huang, W.R. Liu, C.C. Hu,
863 K.R. Lee, J.Y. Lai, Pressure-assisted self-assembly technique for fabricating
864 composite membranes consisting of highly ordered selective laminate layers of
865 amphiphilic graphene oxide, Carbon N. Y. 68 (2014) 670–677.
866 [54] F. Galiano, F. Falbo, A. Figoli, Polymeric Pervaporation Membranes : Organic-
867 Organic Separation, in: O. Visakh, P. Nazarenko (Eds.), Nanostructured Polym.
868 Membr., Scrivener Publishing LLC, Massachusetts, United States, 2016: pp. 281–
869 304.

[55] R.W. Baker, J.G. Wijmans, Y. Huang, Permeability, permeance and selectivity: A preferred way of reporting pervaporation performance data, J. Memb. Sci. 348 (2010) 346–352.

[56] D. Yang, J. Li, Z. Jiang, L. Lu, X. Chen, Chitosan/TiO2 nanocomposite pervaporation membranes for ethanol dehydration, Chem. Eng. Sci. 64 (2009) 3130–3137.

[57] S.D. Bhat, T.M. Aminabhavi, Pervaporation-Aided Dehydration and Esterification of Acetic Acid with Ethanol Using 4A Zeolite-Filled Cross-linked Sodium Alginate-Mixed Matrix Membranes, J. Appl. Polym. Sci. 113 (2009) 157–168.

[58] Y.L. Liu, C.Y. Hsu, Y.H. Su, J.Y. Lai, Chitosan-silica complex membranes from sulfonic acid functionalized silica nanoparticles for pervaporation dehydration of ethanol-water solutions, Biomacromolecules. 6 (2005) 368–373.

[59] M.S. Schehlmann, E. Wiedemann, R.N. Lichtenthaler, Pervaporation and vapor permeation at the azeotropic point or in the vicinity of the LLE boundary phases of organic / aqueous mixtures, J. Memb. Sci. 107 (1995) 277–282.

[60] D. Van Baelen, B. Van Der Bruggen, K. Van Den Dungen, J. Degreve, C. Vandecasteele, Pervaporation of water – alcohol mixtures and acetic acid – water mixtures, Chem. Eng. Sci. 60 (2005) 1583–1590.

Figure 1. Pure cross-linked PVA membrane and its MMMs-GO with 1 wt.% of filler.

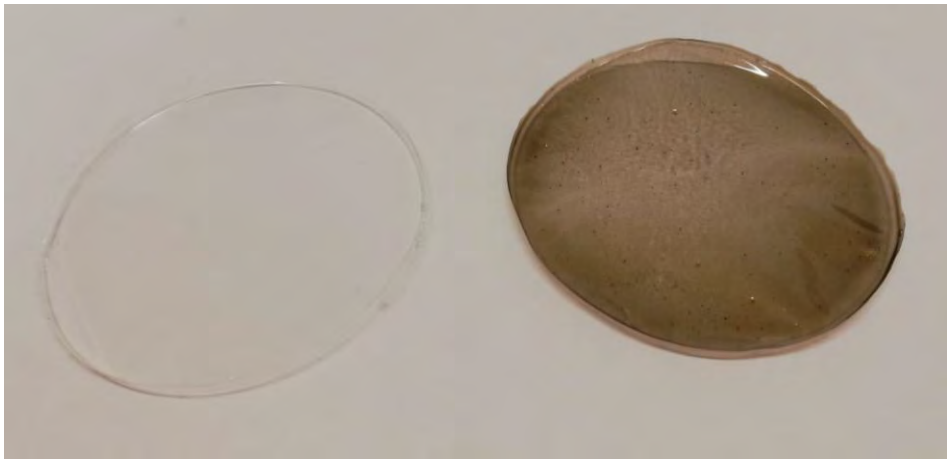

Table 1. T_g and contact angle (CA) values of the pure cross-linked PVA membranes and its MMMs-GO.

Membrane	*T_g (°C)*	*CA (°)*
Pure cross-linked PVA	95.6±2.8	69.6±0.5
Cross-linked PVA + 1 wt.% GO	104.3±0.9	59.9±1.2
Cross-linked PVA + 2 wt.% GO	109.6±1.4	58.4±0.5

Figure 2. Surface and cross-section FESEM images of pure cross-linked PVA (a, b) and MMMs at 1 wt.% (c, d) and 2 wt.% (e, f) GO content, respectively.

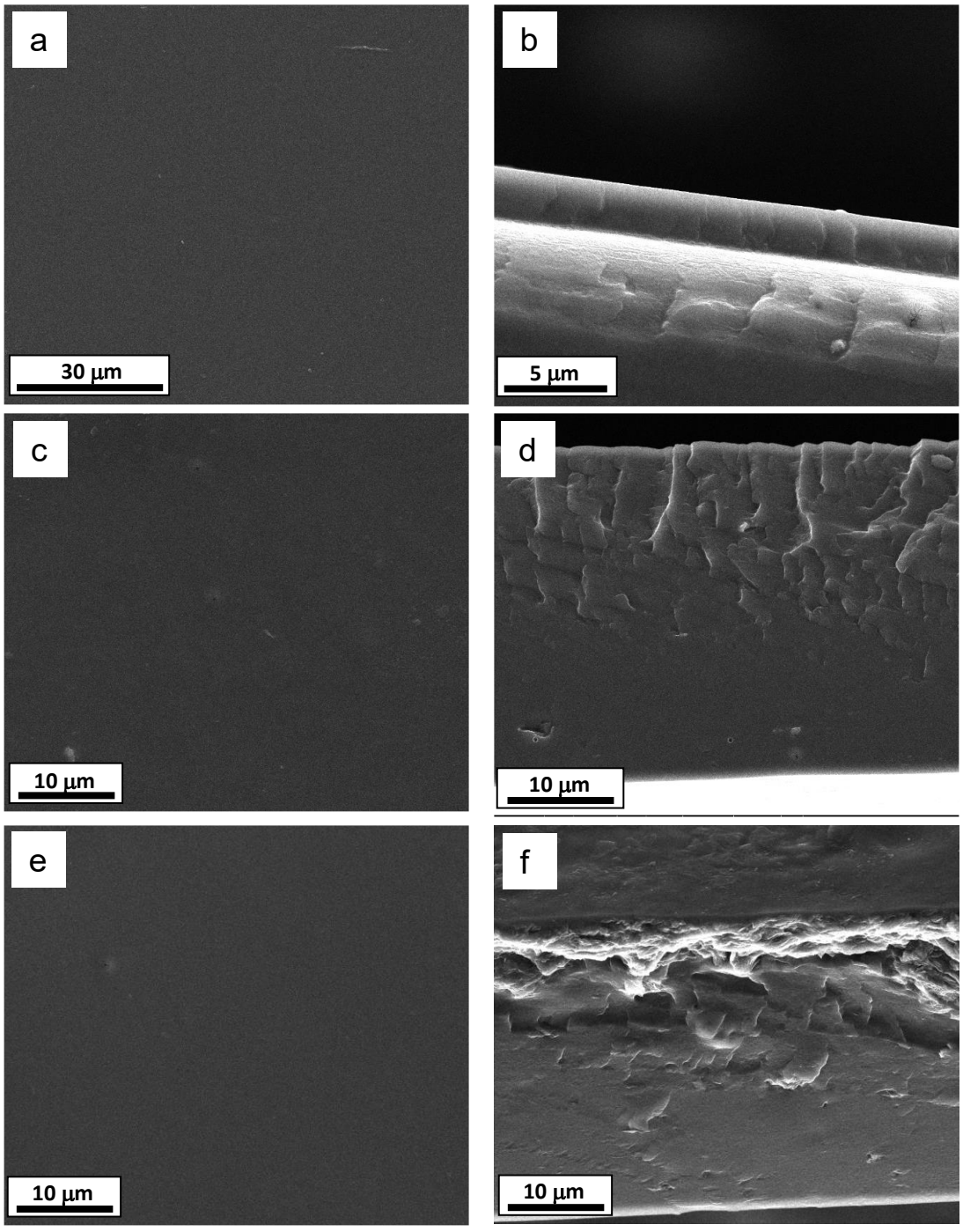

Figure 3. TEM images of GO flakes (a), distribution of GO flakes in MMM (b), GO flake in MMM observed at different angles -26º, 0º and 27º (c), GO flakes in MMM and Fourier transform of the selected zone.

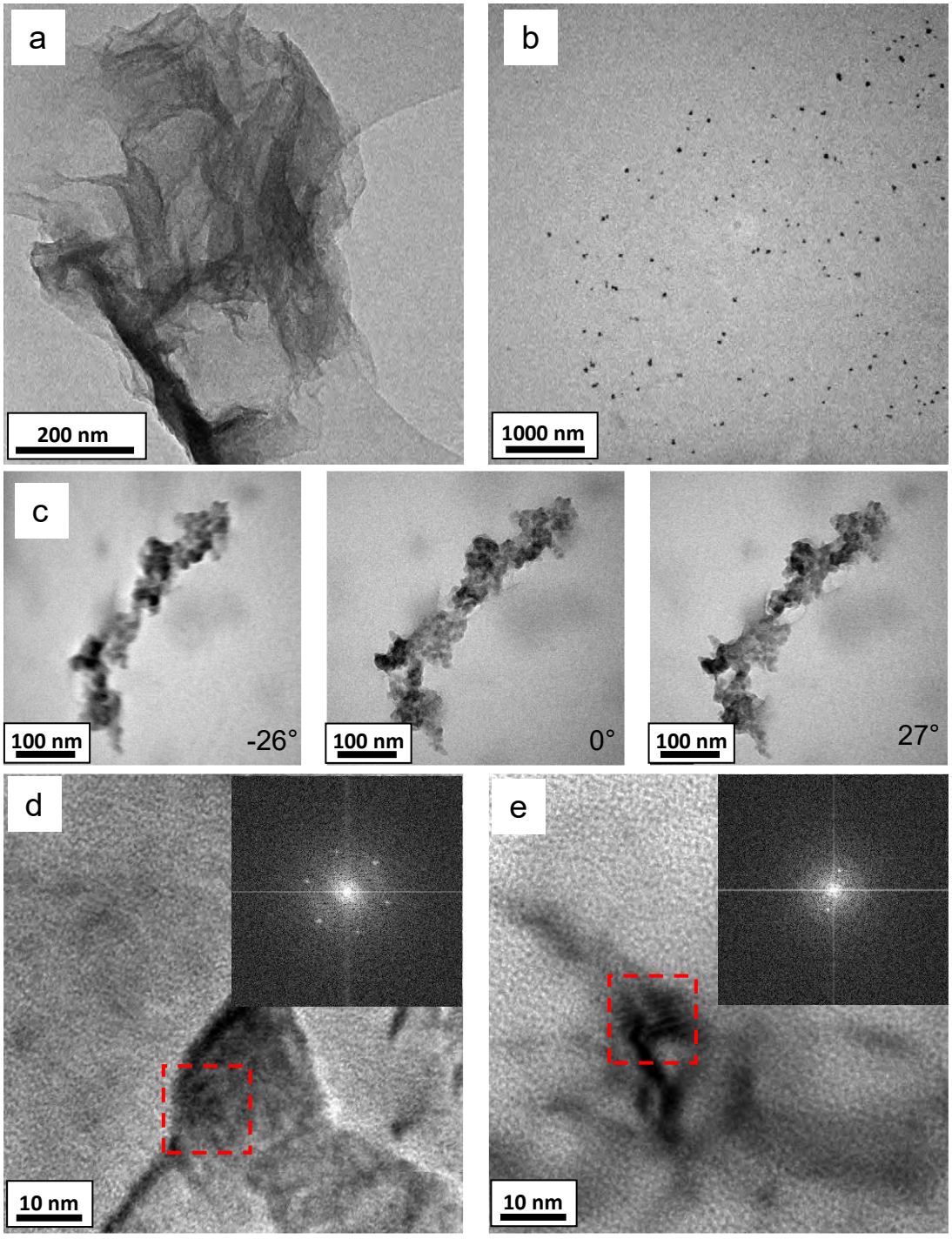

Figure 4. XRD patterns of the pure PVA, pure GO, cross-linked PVA and its MMMs-GO.

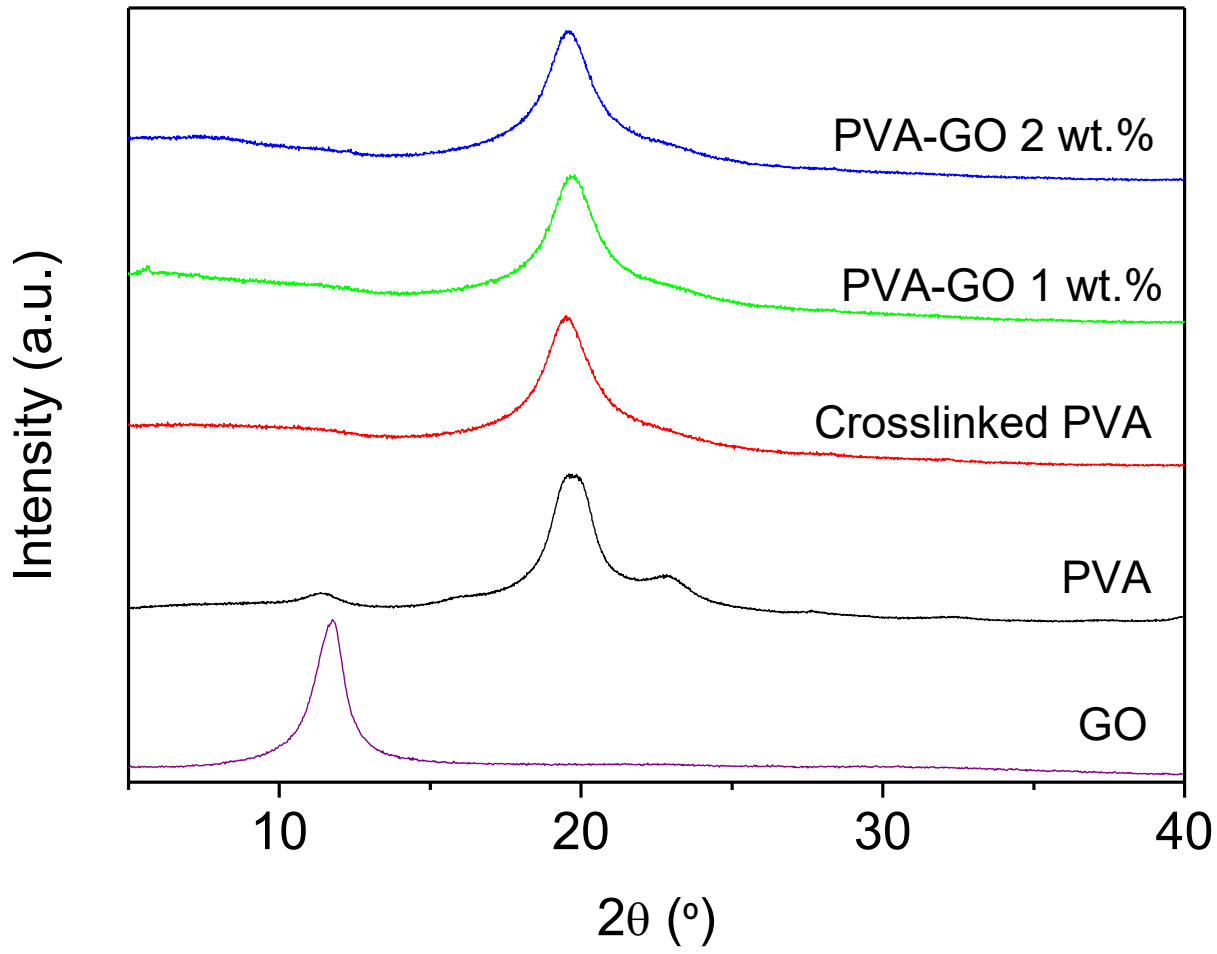

Figure 5. FTIR spectroscopy of the GO, glutaraldehyde, pristine PVA, cross-linked PVA and the PVA-GO 1 wt.% samples.

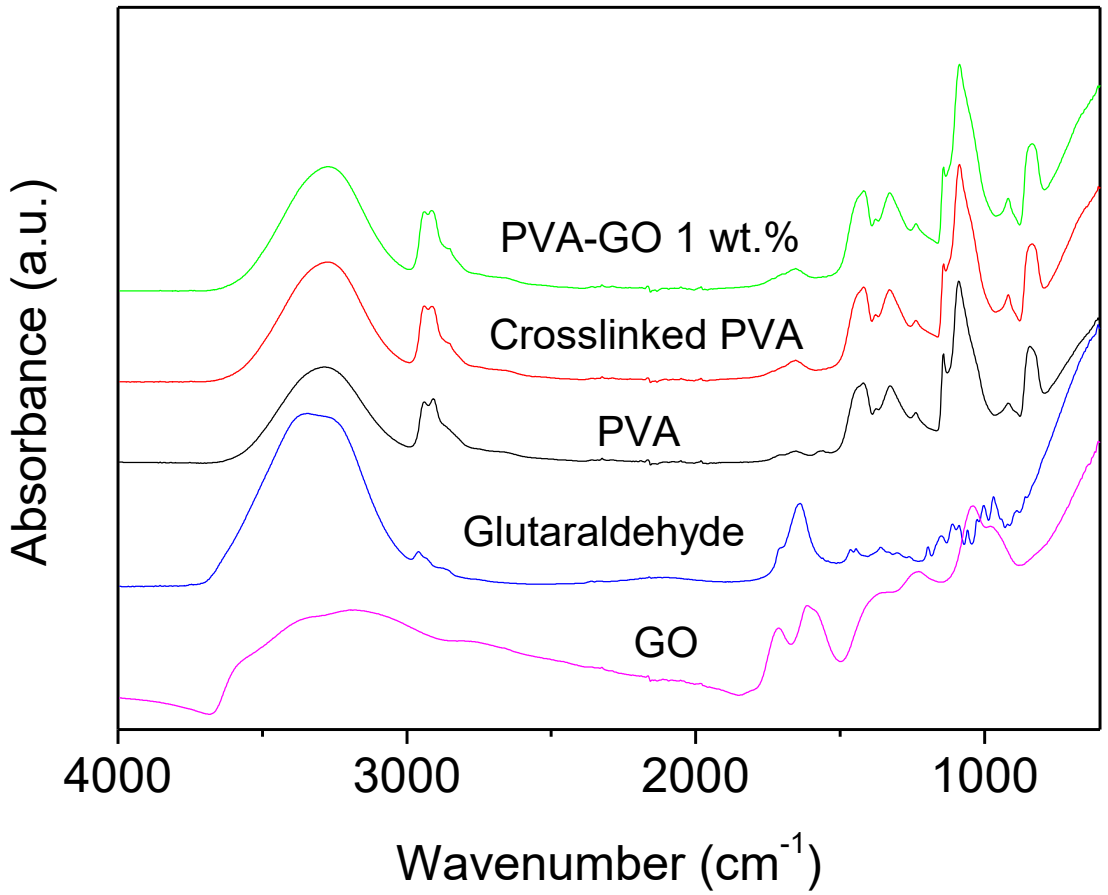

Figure 6. Uptake of the cross-linked PVA membrane and MMMs-GO at 10:90 wt.% water-ethanol (at 40 ºC).

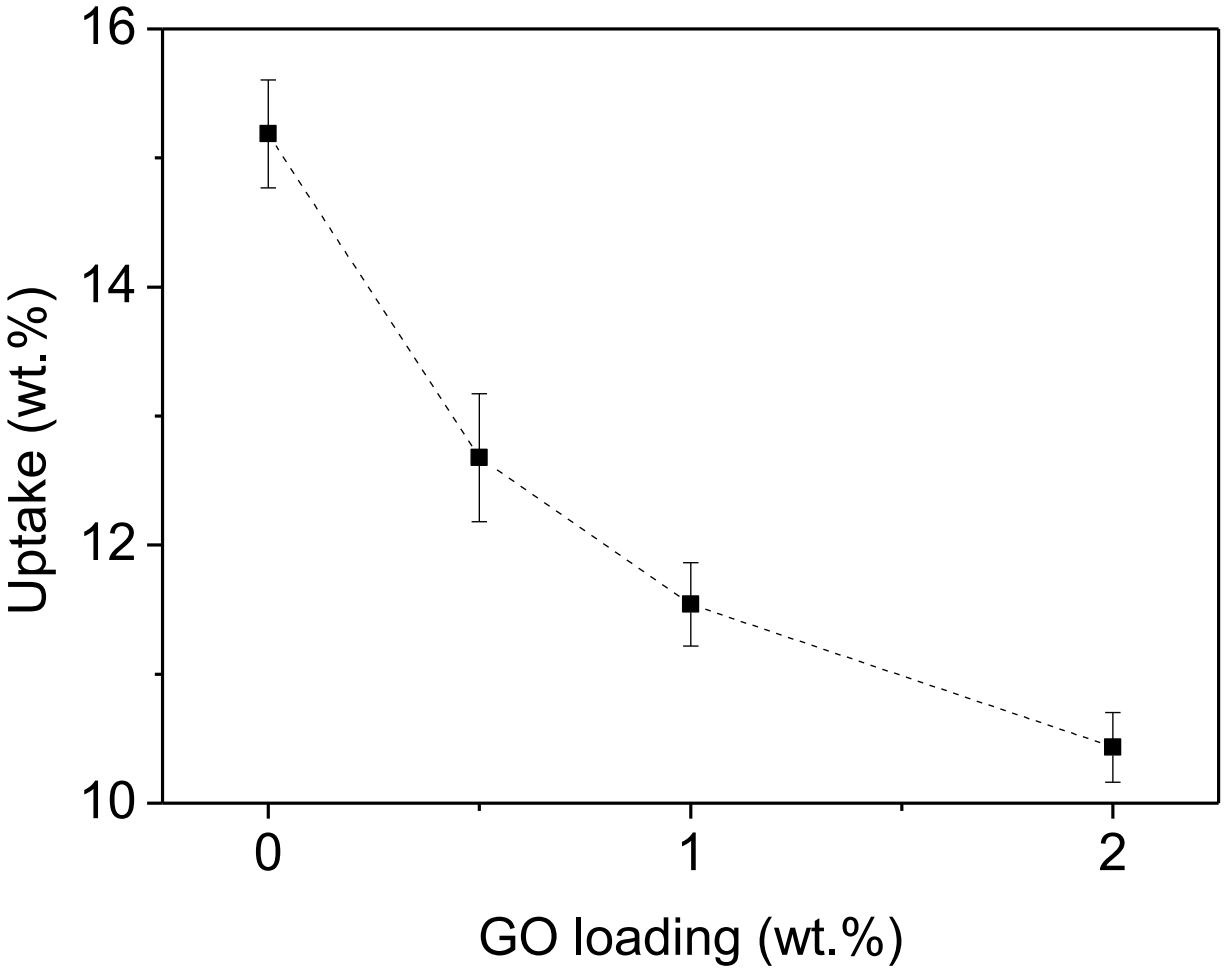

Figure 7. Mechanical properties of cross-linked PVA membrane and MMMs-GO before and after exposure to water-ethanol (10:90 wt.%) mixture.

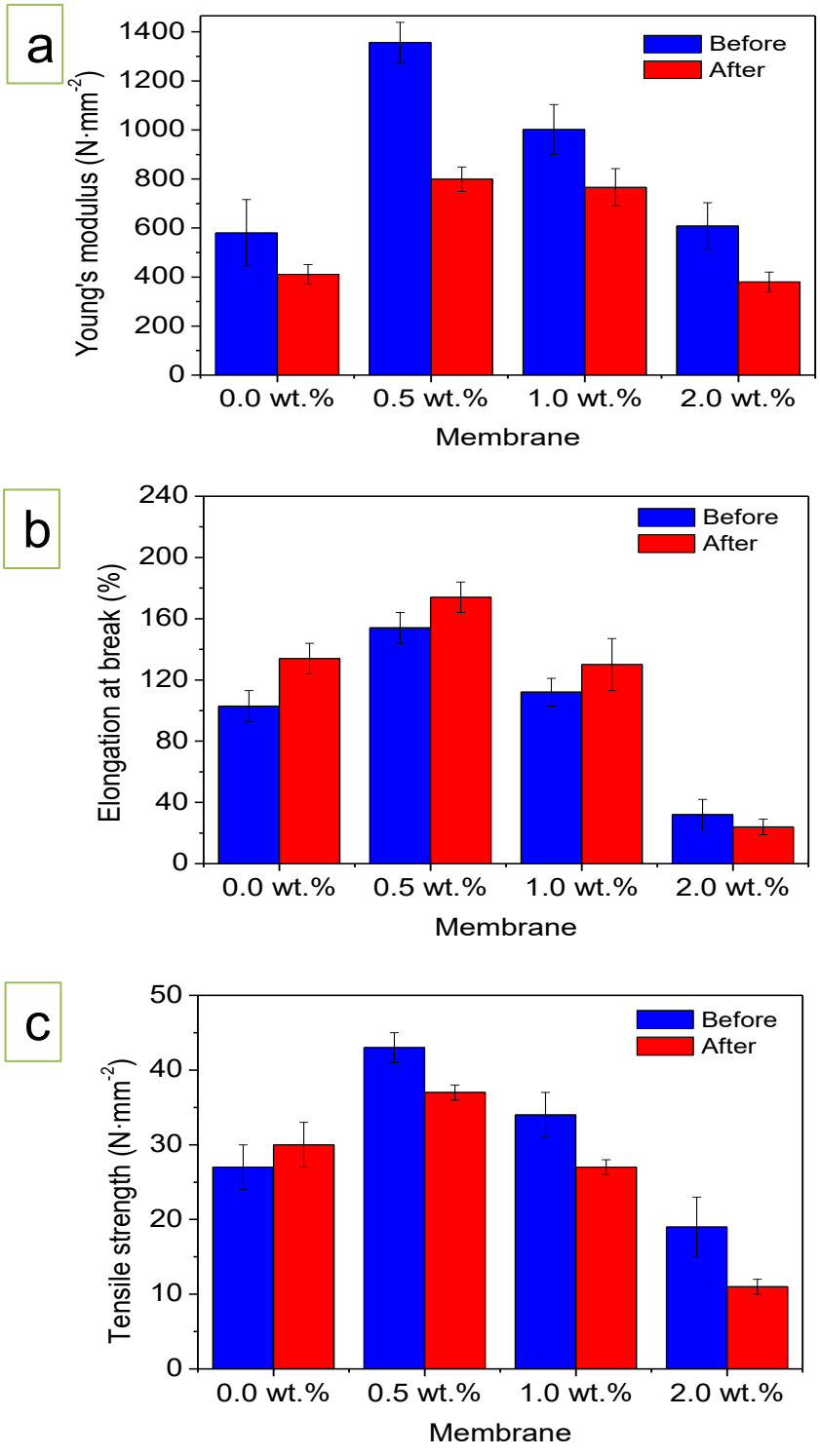

Figure 8. Total permeate flux as a function of the GO loading at different operating temperatures (10: 90 wt.% water-ethanol). The curves are only guides to the eye.

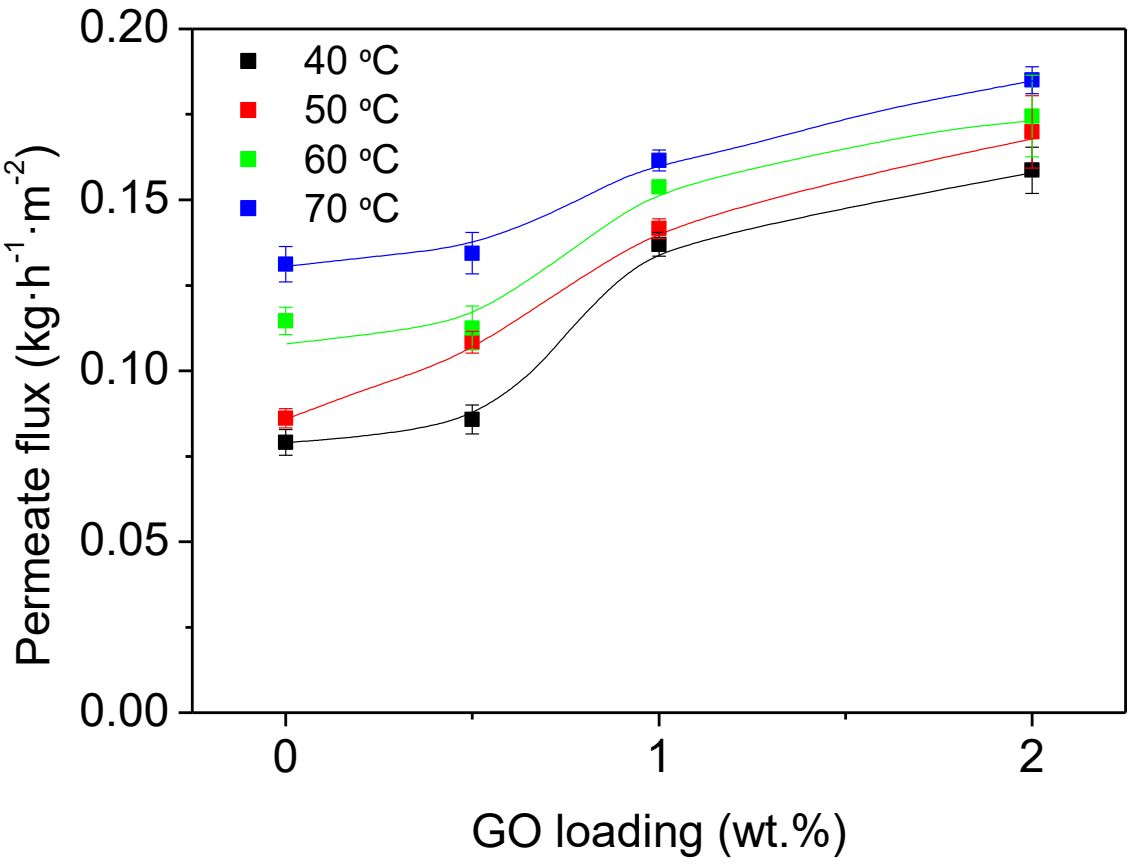

Table 2. Apparent activation energies for total permeate, water and ethanol partial fluxes of the PVA membrane and its MMMs at different GO loadings (Data obtained from **Figures S3-S5**).

	Activation energy values (kJ/mol)		
GO loading (wt.%)	*Total*	*Water*	*Ethanol*
0	7.0	6.5	22.0
0.5	5.3	5.3	17.3
1	2.2	1.6	15.2
2	1.9	0.82	14.1

Figure 9. Separation factor as a function of the GO loading at different operating temperatures (10:90 wt.% water-ethanol). The lines are only guides to the eye.

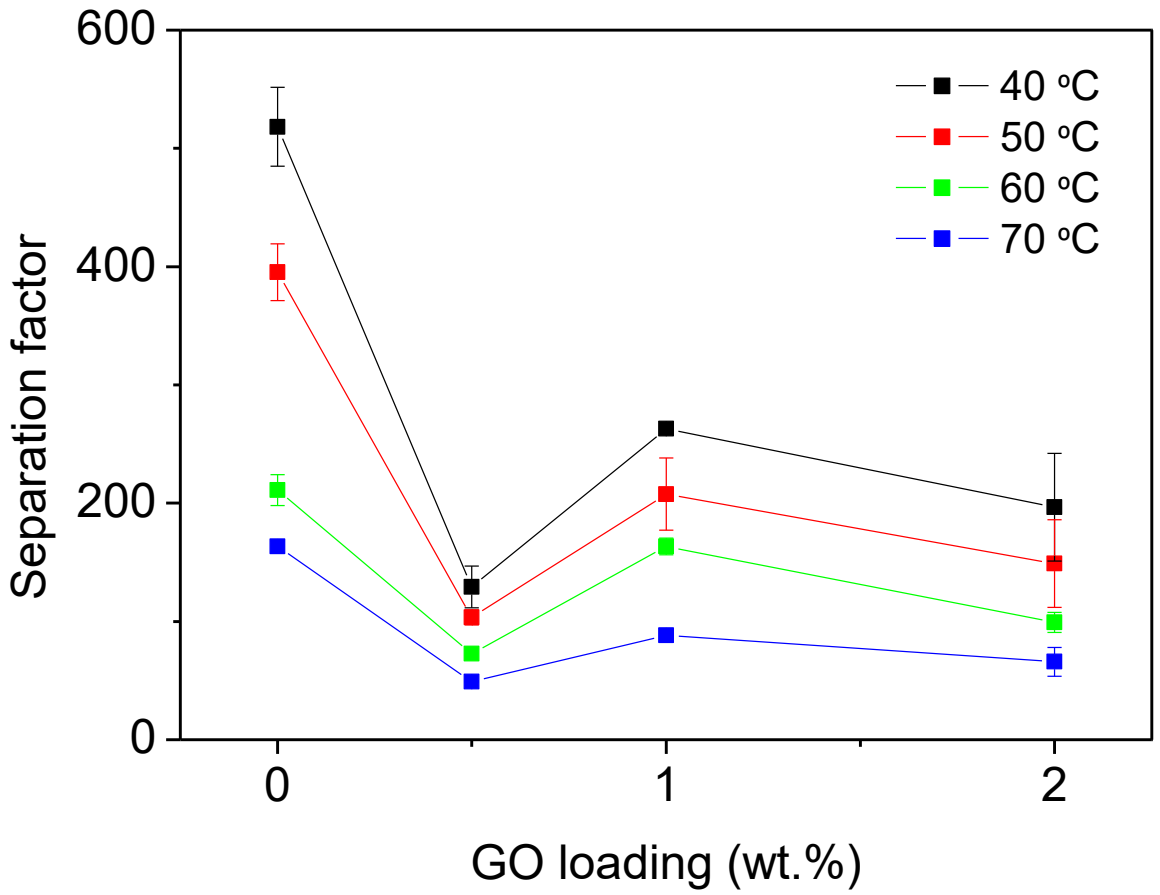

Figure 10. Water and ethanol partial fluxes as a function of the GO loading at different operating temperatures (10:90 wt.% water-ethanol). The curves are only guides to the eye.

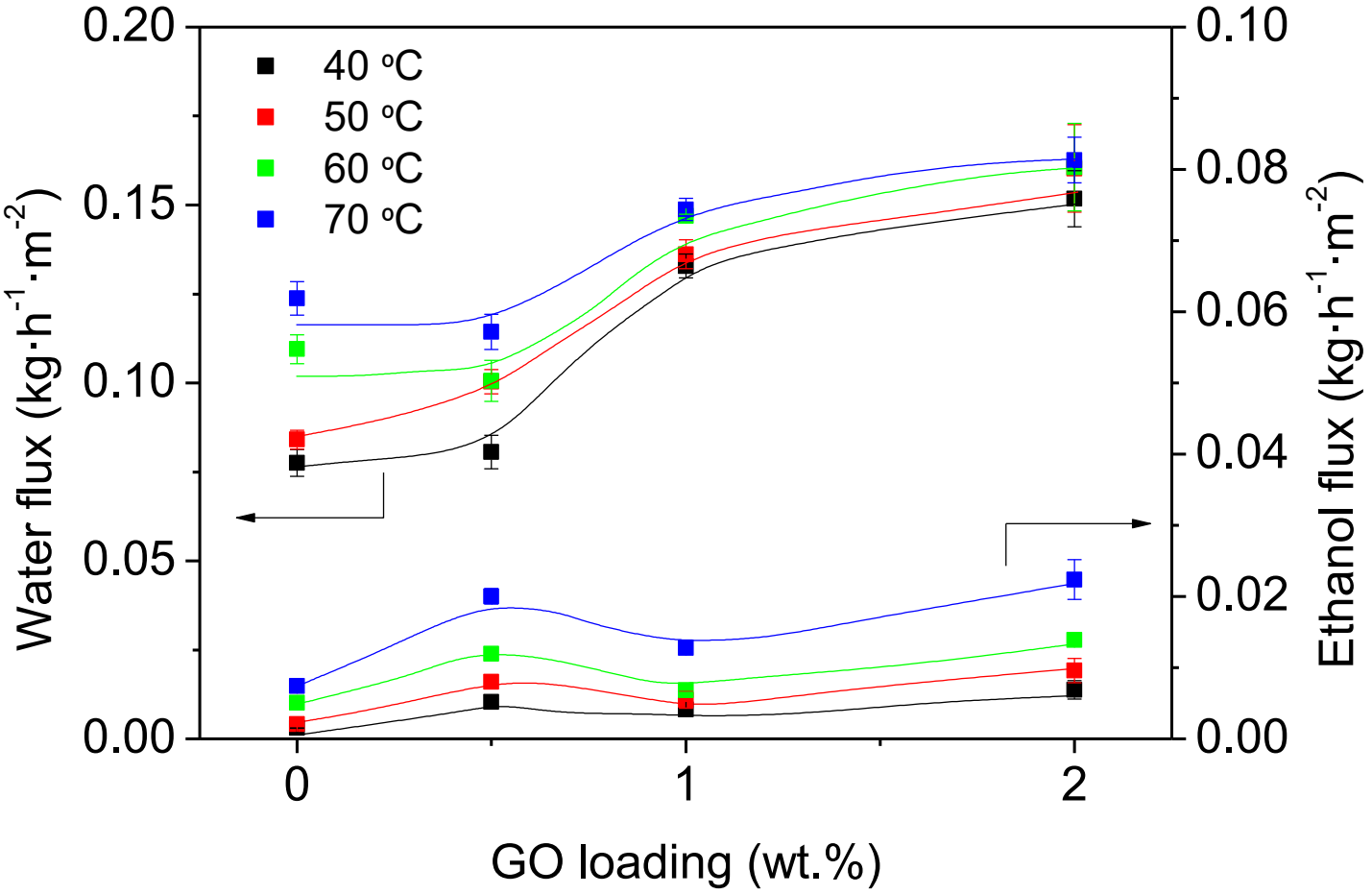

Figure11. Schematic drawing of the hypothetic water permeation mechanism through GO laminates.Inspired by Nair *et al.* [49]

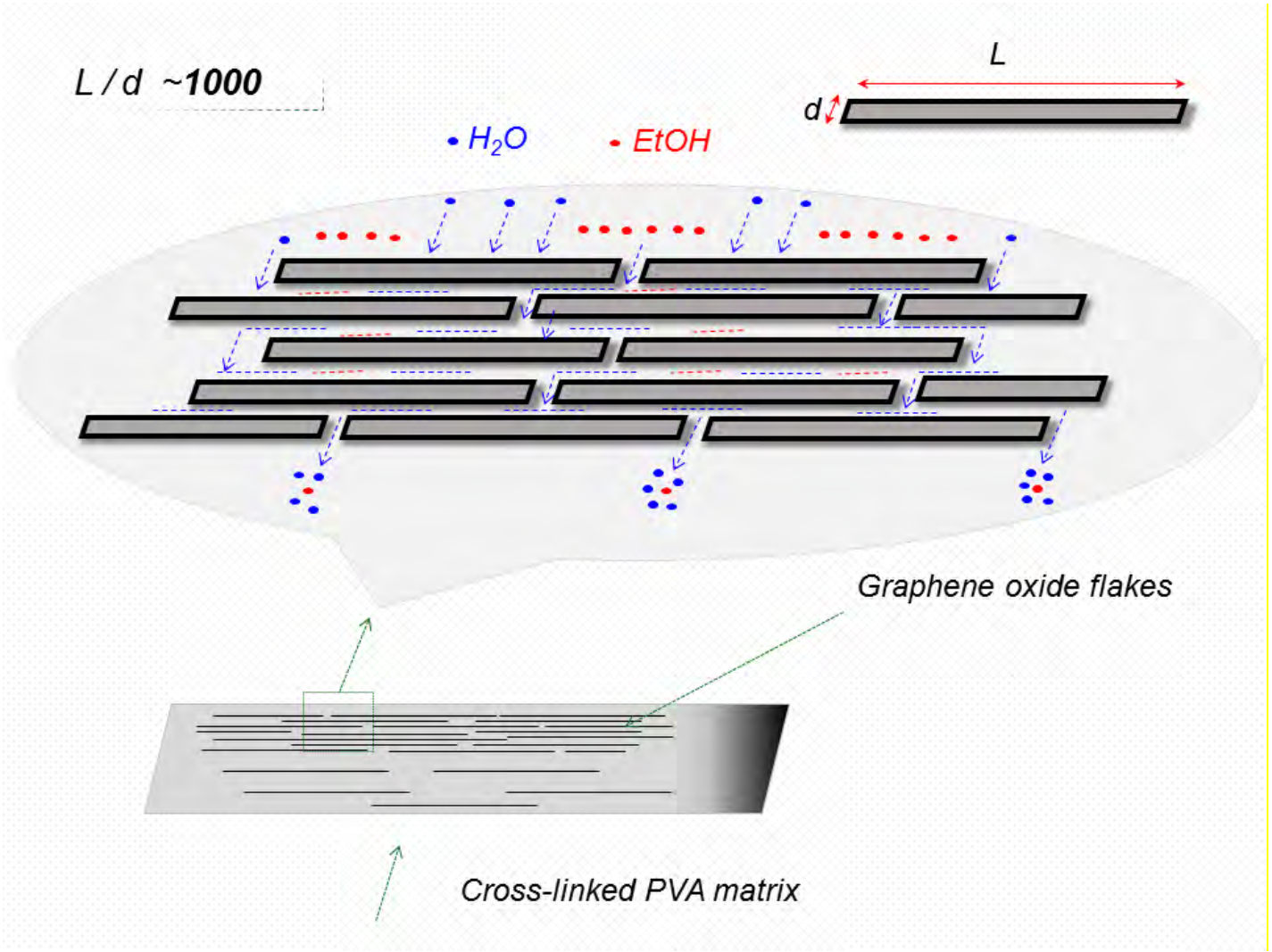

Table 3. Comparison of the cross-linked PVA-GO MMMs performance with other studies for the dehydration of ethanol.

Mixed matrix membrane	Filler loading:	Mixture concentration:	Operating conditions:	J (kg m^{-2} h^{-1})	Separation factor (α)	PSI	Reference:
Cross-linked PVA-filled GO	1 wt.%	10 wt.% H_2O 90 wt.% EtOH	40 ºC, 3 mbar	0.137	263	36.0	This work
Cross-linked PVA-filled GO	2 wt.%	10 wt.% H_2O 90 wt.% EtOH	70 ºC, 3 mbar	0.185	65.9	12.2	This work
Chitosan-filled H-ZSM-5	8 wt.%	10 wt.% H_2O 90 wt.% EtOH	80 ºC, 10 mbar	0.230	152	35.0	[13]
Cross-linked sodium alginate-filled beta zeolite	10 wt.%	10 wt.% H_2O 90 wt.% EtOH	30 ºC, 0.6 mbar	0.130	1600	208.0	[11]
Polyimide-filled ZIF-8	12 wt.%	10 wt.% H_2O 90 wt.% EtOH	42 ºC, 44 mbar	0.260	300	78.0	[6]
Cross-linked sodium alginate-filled beta zeolite	10 wt.%	10 wt.% H_2O 90 wt.% EtOH	30 ºC, 0.6 mbar	0.138	1334	184.1	[57]
PVA-filled MWCNT	5 wt.%	10 wt.% H_2O 90 wt.% EtOH	40 ºC, 1.3 mbar	0.080	500	40.0	[15]

Chitosan-filled TiO_2	6 wt.%	10 wt.% H_2O 90 wt.% EtOH	80 ºC, 50 mbar	0.340	196	66.6	[56]
Polyimide-filled MSS-1	12 wt.%	10 wt.% H_2O 90 wt.% EtOH	42 ºC, 44 mbar	0.310	190	58.9	[6]
Cross-linked chitosan-filled silica	5 wt.%	10 wt.% H_2O 90 wt.% EtOH	70 ºC, 10 mbar	0.410	919	376.8	[58]
Cross-linked PVA-filled ZIF-8-NH_2	7.5 wt.%	15 wt.% H_2O 85 wt.% EtOH	40 ºC, 1 mbar	0.120	200	24.0	[16]
PVA composite membrane (Deutsche Carbone AG/GFT)	-	10 wt.% H_2O 90 wt.% EtOH	60 ºC, 5 mbar	0.140	170	23.8	[59]
PVA composite membrane (PERVAP 2201, Sulzer Chemtech)	-	10 wt.% H_2O 90 wt.% EtOH	60 ºC, 10 mbar	0.100	100	10.0	[60]